CHAPTER 2

Geologic Interpretation of Migrated COCORP Hardeman County, Texas, Seismic Reflection Data: Seismic Expression of a Batholith

ABSTRACT

Focused seismic images of the continental crust were obtained when COCORP's three Hardeman, Texas, lines were migrated with a variable velocity, frequency-domain (F-K) algorithm. Migration of the 16 sec, deep-crustal sections was necessary to collapse diffractions which obscure the underlying signal, and to display dipping energy in its true spatial and temporal position. The interpretation of the migrated data used regional geology, borehole and outcrop data, detailed velocity analyses of the reflection seismic data, and results of previous nearby reflection/refraction work. A well 2.6 km south of Hardeman line 1 reached a basement of 1265±40 m.y. old microgranite porphyry (rhyolite) at 2.86 km (9378 feet, ~1.42 sec). In the Texas panhandle, as much as 1.8 km of rhyolite lavas and tuff (known over 77600 sq km) have been drilled without reaching the underlying plutonic or metamorphic rocks. Granitic intrusions, some contemporaneous with the rhyolite and some older, are found in hundreds of deep oil wells and in outcrop. Precambrian schist and gneiss probably extend regionally underneath the plutonic intrusions.

We adopt Hamilton and Myers' (1967) hypothesis that epizonal batholiths are tabular in shape, spread laterally at shallow (to ~10 km) depth, and may crystallize beneath their own volcanic ejecta, for our interpretation that part of a batholith has been sampled seismically in Hardeman County. Mafic magmas, effective heat transfer fluids for crustal magmatic processes, probably supplied the heat to generate silicic magmas in the lower crust, and also rose in the crust to provide some of the heat needed to keep a tabular upper crustal magma chamber molten long enough to erupt the voluminous volcanics observed. The

close spatial (and perhaps temporal) association of widespread silicic and mafic rocks in the Texas and Oklahoma basement and in outcrop in the Wichita Mountains indicates regional bimodal magmatic activity.

The ~7.5 km thick pluton is interpreted as capped with rhyolitic lavas and ash-flow tuffs, which seismically are intra-basement layered reflectors from 1.42 to ~1.6 sec (~2.86-~3.4 km depth). At greater depth, where porosity in the volcanics is lost, the transition from rhyolitic to granitic rocks is seismically transparent (~1.6 to 2.8 sec, ~3.3-~7.1 km depth). Strong reflections at 2.8 sec and 3.8 sec (~7.1 and ~10.5 km depth) may be tabular mafic bodies ~800 m thick within the rhyolite/granite section and at the base of a tabular granitic pluton, respectively. Several discontinuous reflectors occur within the batholith between 2.8 and 3.8 sec (~6.7 to ~9.8 km depth). The interval velocity here, 6.1-6.5 km/s, indicates a silicic-to-intermediate composition in the lower half of the batholith. The high-amplitude reflections are interpreted as gabbroic underplating; the base of the silicic pluton is clearly defined such that there is ***not*** a gradual downward transition to sub-plutonic rocks. We interpret the two mafic sills as evidence for at least two pulses of bimodal plutonism during the known lengthy, Precambrian magmatic episode (~1260-1100 m.y.a.). Between 4 and 11 sec, under the pluton, are many short, shallowly dipping reflection segments; however, the observable dips at these depths are severely limited by the shortness of the lines. These reflections may represent deformed layers in Precambrian schist and gneiss (migmatite, amphibolite).

INTRODUCTION

The nature of the crust and the crust-mantle interface is an intriguing puzzle that has long challenged geophysicists. Our geophysical knowledge of the continental crust has been based chiefly on gravity, magnetics, seismic refraction, and electro-magnetic methods. For deep-crustal imaging, the resolution of all these methods is on the order of tens of kilometers. Crustal seismic reflection data yield information on the order of ~.1 - 10s of km, offering far more

resolution than other geophysical tools. Such studies can: locate acoustic impedance contrasts, thus identifying lithologic layering and detailed structure on the order of the seismic wavelength; determine velocities, either by (conventional) hyperbola curvature or by focusing and imaging the earth picture by depth migration, thus leading to an understanding of possible crustal lithologies; locate discontinuities such as gently dipping faults (Chapter 3); and help to determine the geometric form of batholiths These data in turn can elucidate tectonic and thermal processes, which are important in locating mineral resources.

Recently COCORP (Consortium for Continental Reflection Profiling) has been gathering 12- and 24-fold VIBROSEIS[1] seismic reflection data. This represents the highest fold coverage (and best signal/noise ratio) to date in deep crustal seismic reflection work. However, all previous interpretations of the COCORP data (Oliver *et al.*, 1976; Oliver and Kaufman, 1977; Smithson *et al.*, 1979; Schilt *et al.*, 1979) have used unmigrated sections, wherein significant diffractions and incorrect spatial locations of dipping energy hindered accurate interpretation. This paper presents an interpretation of the three migrated profiles in Hardeman County, Texas, the first study area of COCORP. Figure 2.1 shows the location of these lines. Petty-Ray Geophysical Co. carried out the field work and processing. Data collection and processing procedures are described in the appendices.

There were several outstanding incentives to study, migrate, and interpret these interesting deep crustal sections. First, the seismic sections consist of mostly basement rocks, which provides an excellent opportunity for studies of the crystalline crust. The Pan American (Amoco) No. 1 Bestwall Gypsum well, 2.56 km south of line 1 (Figure 2.1), encountered micrographic microgranite porphyry (rhyolite) at 1.42 sec (2.856 km). The well's sonic and seismic velocity survey provide the time-to-depth conversion, and RMS and interval velocities for this study. A rhyolite core sample was dated at 1265±40 m.y. (Oliver, *et al.*, 1976). Below 1.42 sec to ~11 sec, the rocks in the

[1]Registered trademark, Continental Oil Co.

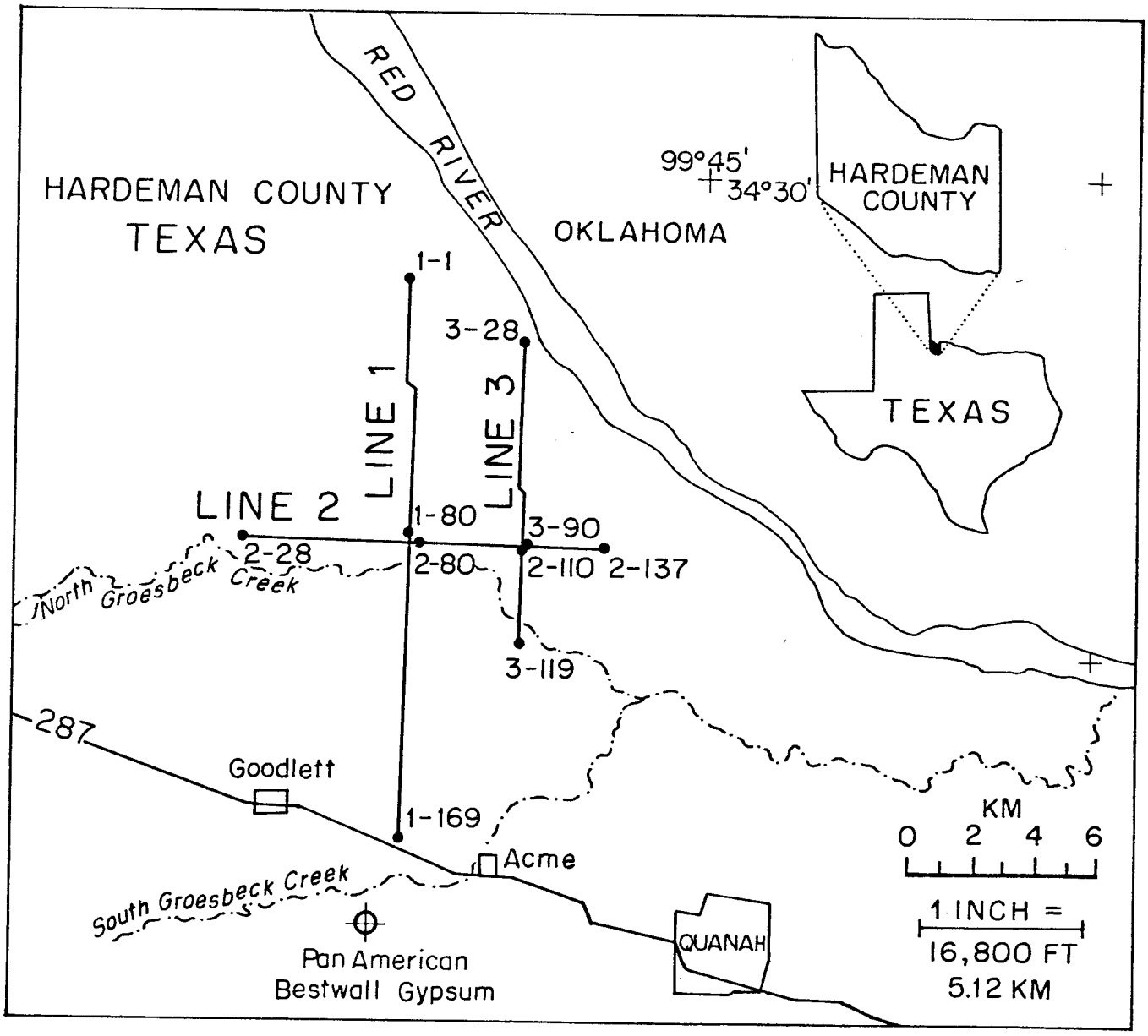

FIG. 2.1. Basemap for COCORP Hardeman Cty., Tx., data. The Pan Am. Bestwall Gypsum well with sonic 2.56 km south of line 1 reached basement (rhyolite) at 1.4 sec (2.9 km, 9400 ft).

seismic section are presumably similar to the igneous and metamorphic basement rocks known regionally by borehole and outcrop data. Second, there are many basement reflections on the unmigrated data, which indicate that the signal-to-noise ratio is high enough to warrant migration.

Third, there is very good penetration of relatively high frequencies to deep within the basement. The expected maximum frequency content of the reflected energy can be estimated by the simple relation

$$Q = t\,f$$

where Q is an average quality factor of the crust, t is two-way traveltime, and f is the frequency in Hz. Assuming an average crustal value of 200 for Q, frequencies on the order of 20 Hz can be expected at 10 sec. Some 25 Hz signal is seen at 10 sec, which indicates that Q may be higher than 200. The higher-frequency content yields better resolution. The start of crystalline basement at 1.42 sec probably helped in the transmission of deep-crustal "high" frequencies.

The migration of these deep seismic profiles is necessary to collapse the numerous diffractions and shift the dipping reflections to their correct spatial and temporal positions. Migration can be accomplished by a variety of algorithms. The frequency-domain time-variable-velocity migration algorithm, as described by Stolt (1978), was used to migrate the data presented in this paper. The migrated sections provide more accurate and more detailed images of the continental crust.

BRIEF REVIEW OF THEORY AND POST-STACK PROCESSING

The frequency-domain time-variable-velocity algorithm has three main steps (Stolt, 1978). Because the frequency-domain migration is rigorously correct only for a constant-velocity medium, the stacked section is first rescaled in the time domain to make it appear as if it were a constant-velocity section. "Stretching" to a pseudo-time

(constant-velocity) domain is based upon an estimate of the RMS velocity function, using the equation

$$t \rightarrow t_n = \sqrt{\frac{2}{\bar{v}} \int_0^t dt\, t\, v_{RMS}^2} \qquad (2.1)$$

where t is time, t_n is the new time coordinate, v_{RMS} is the time-variable RMS velocity, and $\bar{v}$ is an arbitrary constant velocity chosen such that t_n and t are about equal. The dataset is migrated in the frequency domain by mapping and rescaling the two-dimensional Fourier transform of the data, using the equation

$$A_{mig}(k_x,\omega') = vk_z\left[k_x^2 + k_z^2\right]^{-\frac{1}{2}} A\left[k_x,\omega = v\left(k_x^2 + k_z^2\right)^{-\frac{1}{2}}\right] \qquad (2.2)$$

where A_{mig} = the migrated data in the frequency domain, k_x = the spatial wavenumber, ω and ω' = the unmigrated and migrated temporal frequencies, v = migration velocity, k_z = the depth wavenumber, and A = the Fourier-transformed time section which is the input to migration. After migration, the dataset is "unstretched" from the pseudo-time domain back to a true time (depth).

A post-migration gain correction is also performed. Migration is equivalent to collapsing a hypothetical diffraction hyperbola to a (migrated) output point, and on very deep seismic sections, there are noticeable energy losses due to hyperbola truncation near the lower section boundaries. A migration gain correction normalizes the partial hyperbola to the strength of a full hyperbola everywhere on the section. To obtain the appropriate gain, we first recognize that the amplitude of a point scatterer diffraction, $a(\theta)$, as a function of observation angle from the vertical, is given by

$$amp(\theta) = \cos\theta = z\left[\Delta x^2 + z^2\right]^{-\frac{1}{2}}, \qquad (2.3)$$

$$\theta < \left(-\frac{\pi}{2}, +\frac{\pi}{2}\right)$$

where Δx is the distance from the hyperbola top, and z is depth. Integrating the amplitude along a hyperbola, we obtain the following normalization formula,

$$n = \Delta x_L \left[\Delta x_L^2 + v^2 t^2\right]^{-\frac{1}{2}} + \Delta x_R \left[\Delta x_R^2 + v^2 t^2\right]^{-\frac{1}{2}} \qquad (2.4)$$

where the diffraction point is at (x,t) and Δx_R and Δx_L are the distances from the right and left sides of the section to the point.

There are many advantages of the Stolt-stretch F-K migration algorithm It is very amenable to a minicomputer, it is fast, and it is easier to keep stable than its time counterpart. The constant velocity F-K algorithm is accurate for all dips up to those which are spatially aliased.

The disadvantages of the V(t) F-K migration algorithm is that by performing the "stretch" (an approximation), accuracy is lost at the higher dips. Also, in theory, there is no change in velocity laterally (i.e., "no dips"). In practice, slight lateral velocity changes and dipping events cause little concern for the accuracy of the output section Rapid variation in velocity either laterally ***or*** vertically can cause problems; if ***both*** occur, problems (inaccuracies) will certainly result. If necessary, the stretching function can be changed along the line to approximate slow lateral velocity variations. Since the thin lens term (or "shifting term") (Claerbout, 1976) cannot be included in these frequency-domain migrations, F-K migrations where the RMS velocity function changes along the line will yield only approximately correct results. In the Hardeman County dataset, one velocity function adequately describes the essentially stratified media so that frequency-domain migration is valid.

The periodic boundary conditions of the frequency-domain migration "wrap" energy "around" the migrated section as the energy migrates up dip. In order not to have "wraparound" obscuring the signal, zero traces were appended (padded) onto the edges of the sections before migration in order to absorb the migrating energy. Each profile was padded out to 1024 traces, which is 200%-500% padding, depending on the

original line length. The steeply dipping reflections seen on the unmigrated sections are not seen on the migrated sections because the energy has moved updip off the ends of the line.

OBSERVATIONS FROM THE DATA

The Reprocessed Stacks

Initial processing was done by Petty-Ray (A, Figures 2.2-2.4). The data were carefully reprocessed by Steve Schilt and George Long of Cornell Univ. (B, Figures 2.2-2.4). Different processing yielded additional insights into the nature of the crust. Both sets of processing were migrated (Figures 2.2-2.7). The reprocessing used better stacking velocities and less severe gating (muting) of the gathers which allowed more signal to enter the stack and improved the sedimentary section stack (cf. location A, Figure 2.5). The new velocity functions match the well velocities (0-1.4 sec) far better than the old stacking velocities. The comparison of the two high-amplitude events (at 2.8-3 sec and 3.8 sec, Figures 2.2-2.5) on the "before" and "after" sections reveals a shorter wavelet after reprocessing which can be attributed to a more effective deconvolution. (Compare locations B and C, Figure 2.5, with their reprocessed equivalents.) Significant diffractions are also seen on the data (D, Figure 2.5; arrow, Figure 2.6). The improvement in processing enhanced the data and added badly needed velocity information.

The reprocessing reduced the amplitude contrasts between different zones on the data and obscured some previous insights (A, B, Figure 2.2). In particular, the "transparent" nature of the 1.6-2.8 sec zone and the heterogeneous nature of the rocks below 3.8-4.0 sec seen clearly on the earlier sections (Figures 2.2A, 2.3A, 2.4A) are not as obvious on the reprocessed sections (Figures 2.2B, 2.3B, 2.4B). The amplitude "homogenizing" probably resulted from the AGC and/or the post-stack filtering.

The True Amplitude CDP Gathers

The strong reflections beginning at about 2.8 and 3.6-3.8 sec on the AGC'd stacked data appear to be fairly continuous laterally at first glance (Figures 2.2-2.4). Closer scrutiny suggests lensoid or discontinuous reflectors, as on the first third of line 2 (Figure 2.3), and the first third of line 1 (Figure 2.2).

The true amplitude CDP gathers (Figure 2.8) reveal that these two events are the strongest reflections in the dataset, much higher in reflectivity than the sedimentary horizons, and ***highly*** variable in amplitude laterally. The deeper event (at ~3.8 sec) is more typically the stronger. 0.5-2.5 km is the average lateral extent of the higher-amplitude reflectors.

The Migrated Sections

Of the three Hardeman lines, lines 2 and 3 were only 11 km long, line 1 only 17 km, and the longest offset (the cable length) was 5.18 km. The shortness of the cable length and the lines frustrated accuracy in the velocity estimations, limited the dips recorded, and hindered interpretation. The observable dips on migrated Hardeman lines, as a function of line length and maximum recording time available for migration, were calculated (Chapter 1). It was shown that the length of line is the limiting parameter, not recording time. In the center 8 km of line 1, 20-degree dip (either sense) is obtainable to 4.2 sec (~12 km), 10-degree dip (either sense) is obtainable to 8.7 sec (~26 km), and 5- degree dip (either sense) to 14.8 sec (~44 km). Knowing these dip limitations the middle 8 km of line 1 can be used to describe the seismic nature of the continental crust at Hardeman County. The shortness of lines 2 and 3 so severely limit the dip recordable that the center 9 km of the migrated sections are useful only for 0-10 degree dips to 3.3 sec (~10 km), 5-degree dips to ~7 sec (20 km), and less than 5-degree dips to 14.8 sec (~44 km). Even though the data is dip-limited, useful geologic information about the crust can be extracted.

FIG. 2.2. Line 1. All seismic sections are ~1:1. A) Initial processing, common-depth-point (CDP) stack. Arrow points to a dipping event that moves ~25 km laterally upon migration. B) Reprocessed CDP stack. C) F-K (frequency domain) migration of reprocessed stack. Note how dipping events move in space and time.

FIG. 2.3. Line 2. A) Initial processing, CDP stack. B) Reprocessed CDP stack. C) F-K migration of initial-processing CDP stack. D) F-K migration of reprocessed CDP stack.

FIG. 2.4. Line 3. A) Initial processing, CDP stack. B) Reprocessed CDP stack. C) F-K migration of initial-processing CDP stack. D) F-K migration of reprocessed CDP stack.

FIG. 2.5. Comparison of initial and reprocessed CDP stacks of line 2. The reprocessed sections had less severe mutes and better sedimentary velocities (note improvement at A). A more effective deconvolution in reprocessing enhanced the reflectors at B and C. Arrow D indicates a diffraction, which will be collapsed to a point (offsection) after migration.

FIG. 2.6. Line 1: 17 km length, 15 sec displayed. ~1:1. Reprocessed CDP stack. The reflection at A moves ~5 km laterally to the left (see location A, Figure 2.7). The arrow points along diffractions which collapse (disappear) upon migration.

FIG. 2.7. Line 1: F-K migration of the reprocessed stack. Note migrated position of reflector A (compared to Figure 2.6). B is a zone of seismic transparency, perhaps a "homogeneous pluton". C is a zone of high reflector density, perhaps a zone of recumbently folded layers or fortuitously gently-dipping-to-horizontal foliation in schist or gneiss. D is an area of convergent dips, possibly a recumbent fold.

FIG. 2.8. True amplitude CDP gathers. A. Line 3. The start of each gather is marked at the top. Offset increases to the left in each gather. Maximum offset is 5.18 km. Both horizons (2.8 and 3.8 sec) are highly reflective, stronger than the sedimentary reflections. The 2.8 sec event decreases in amplitude to the right. The nearest offset is tagged. B. Line 1. Only the 3.8 sec horizon is high amplitude. Note the decrease in amplitude toward the right. Offset increases to the left. The nearest offset is tagged. C. Line 2. The reflectivity of the two high-amplitude horizons varies along the line. The nearest offset is tagged.

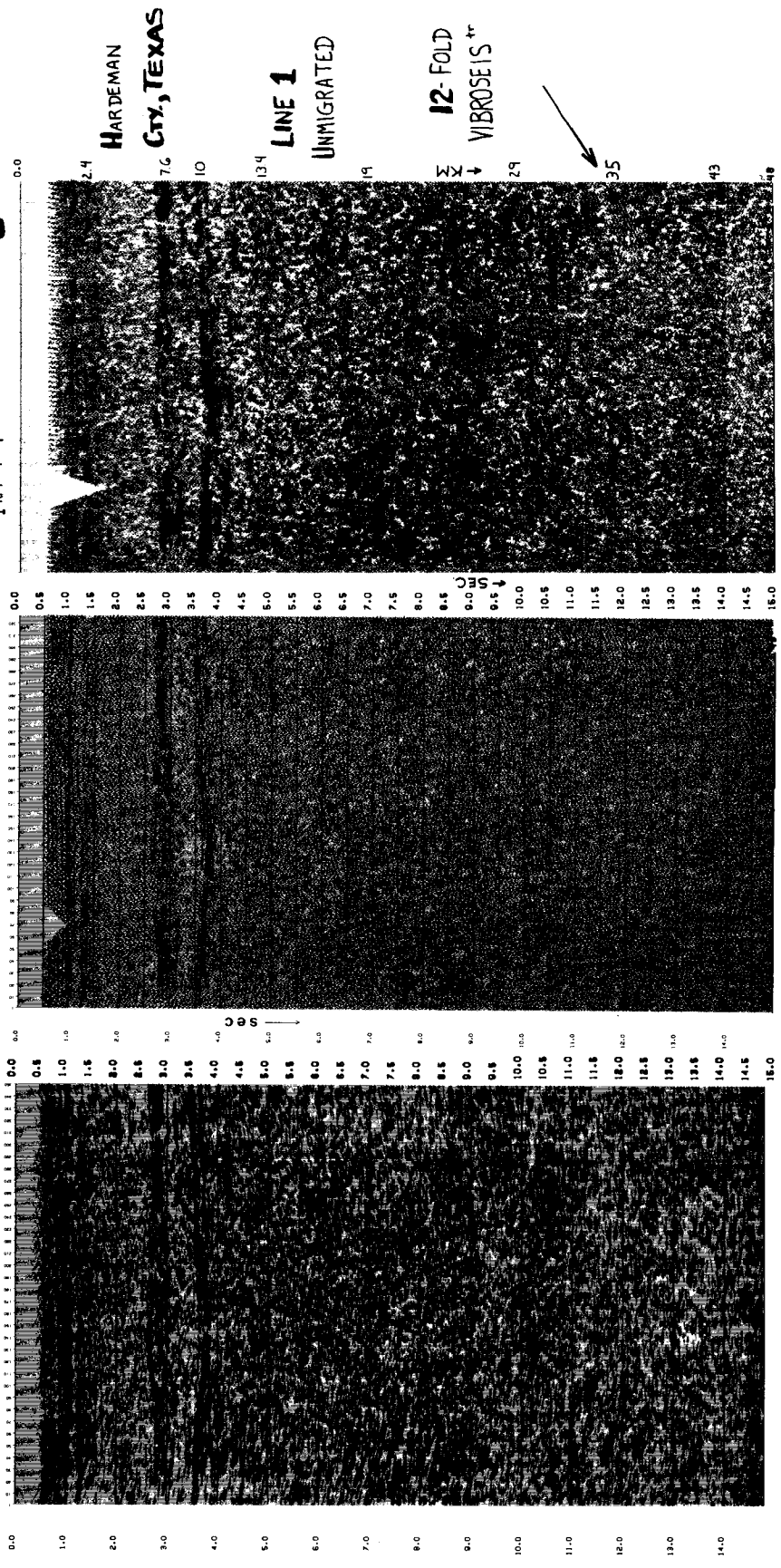
S
1 KM
HARDEMAN
CTY., TEXAS
LINE 1
UNMIGRATED
12-FOLD
VIBROSEIS
SEC
A
B
C

FIG. 2.2.

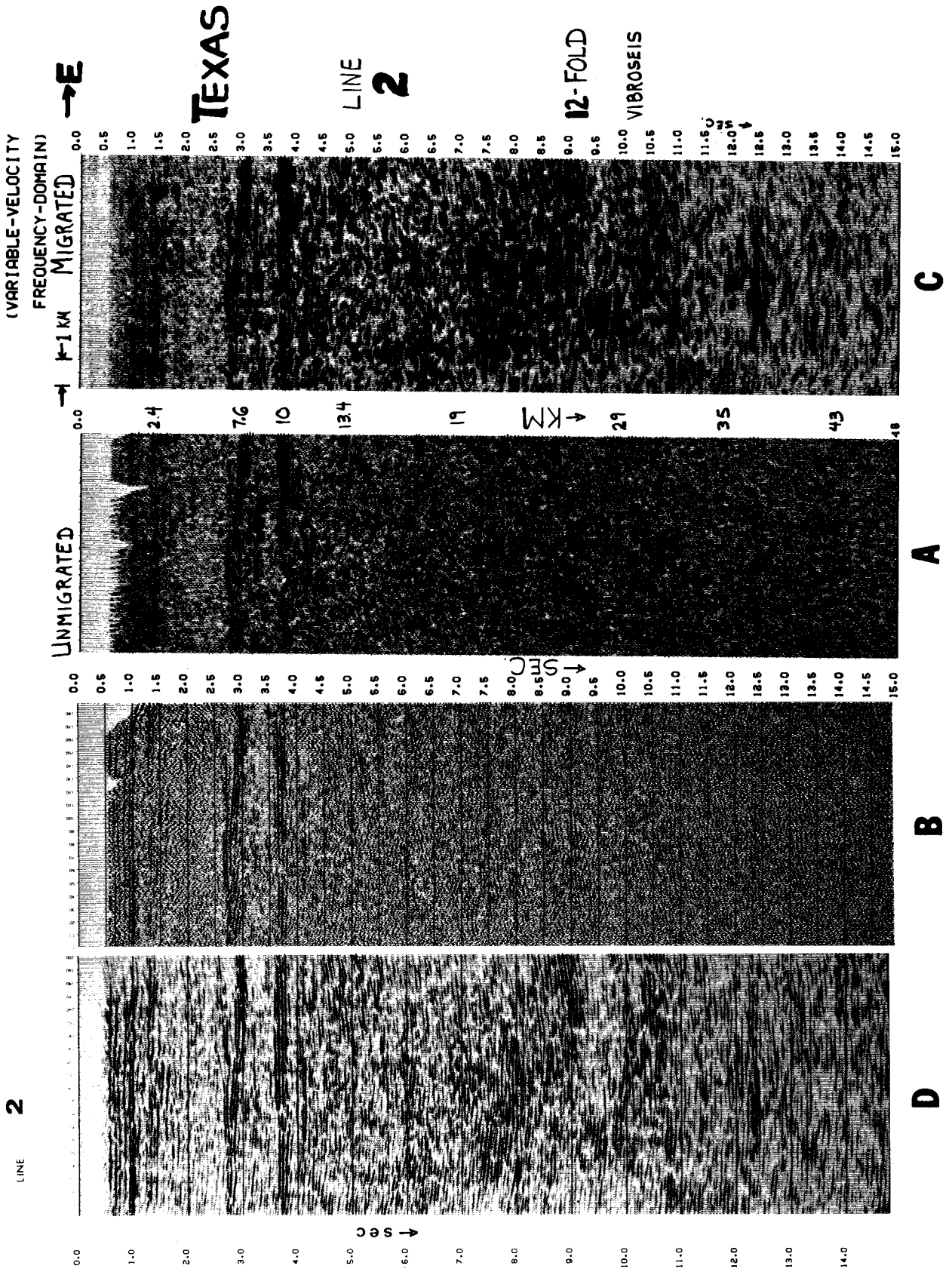
(VARIABLE-VELOCITY FREQUENCY-DOMAIN)
MIGRATED
UNMIGRATED
TEXAS
LINE 2
12-FOLD VIBROSEIS
LINE 2
A
B
C
D
E
KM
sec

FIG. 2.3.

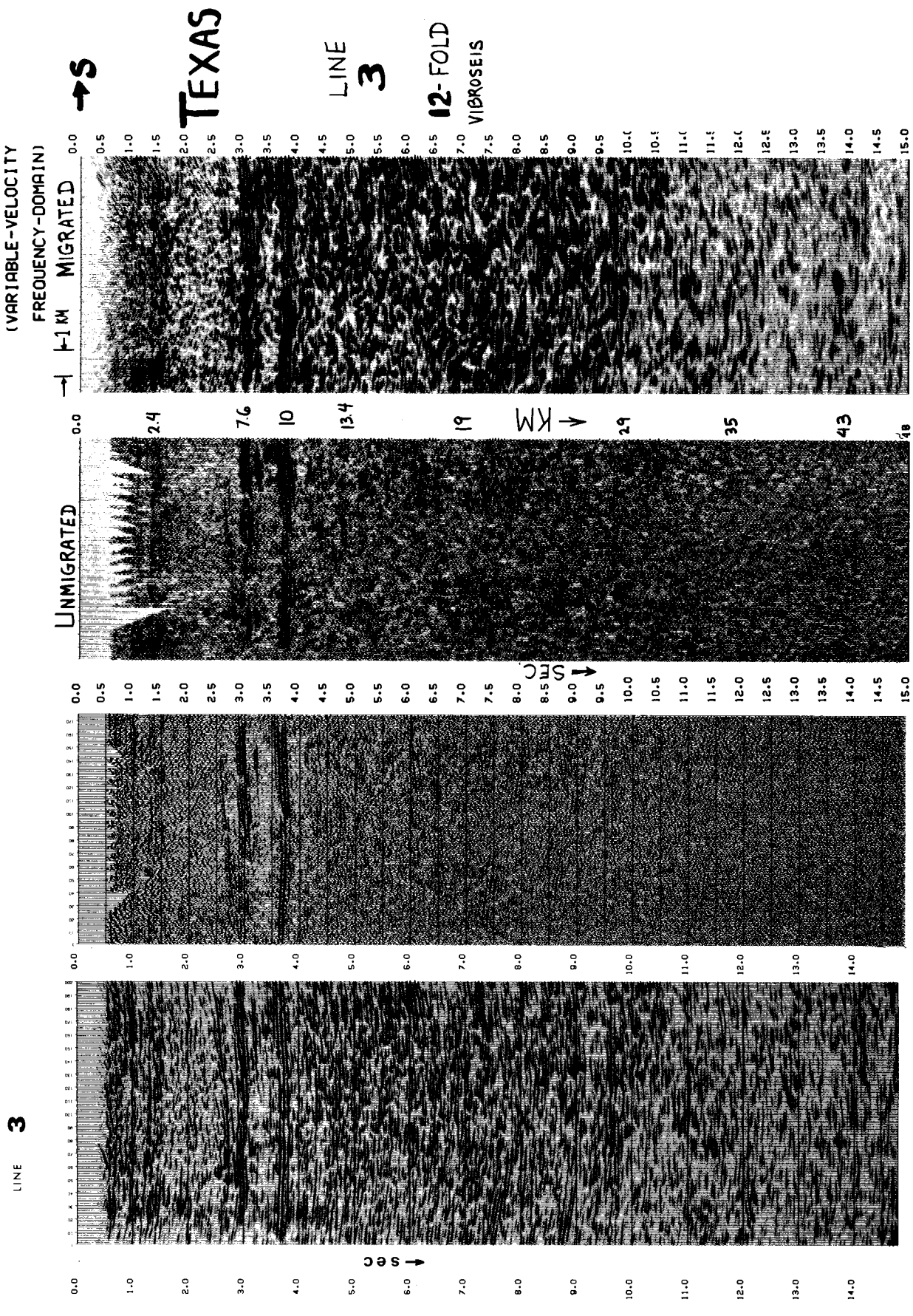
(VARIABLE-VELOCITY
FREQUENCY-DOMAIN)
MIGRATED
1 KM
S
TEXAS
LINE
3
12-FOLD
VIBROSEIS
UNMIGRATED
KM
SEC
LINE 3
A
B
C
D

FIG. 2.4.

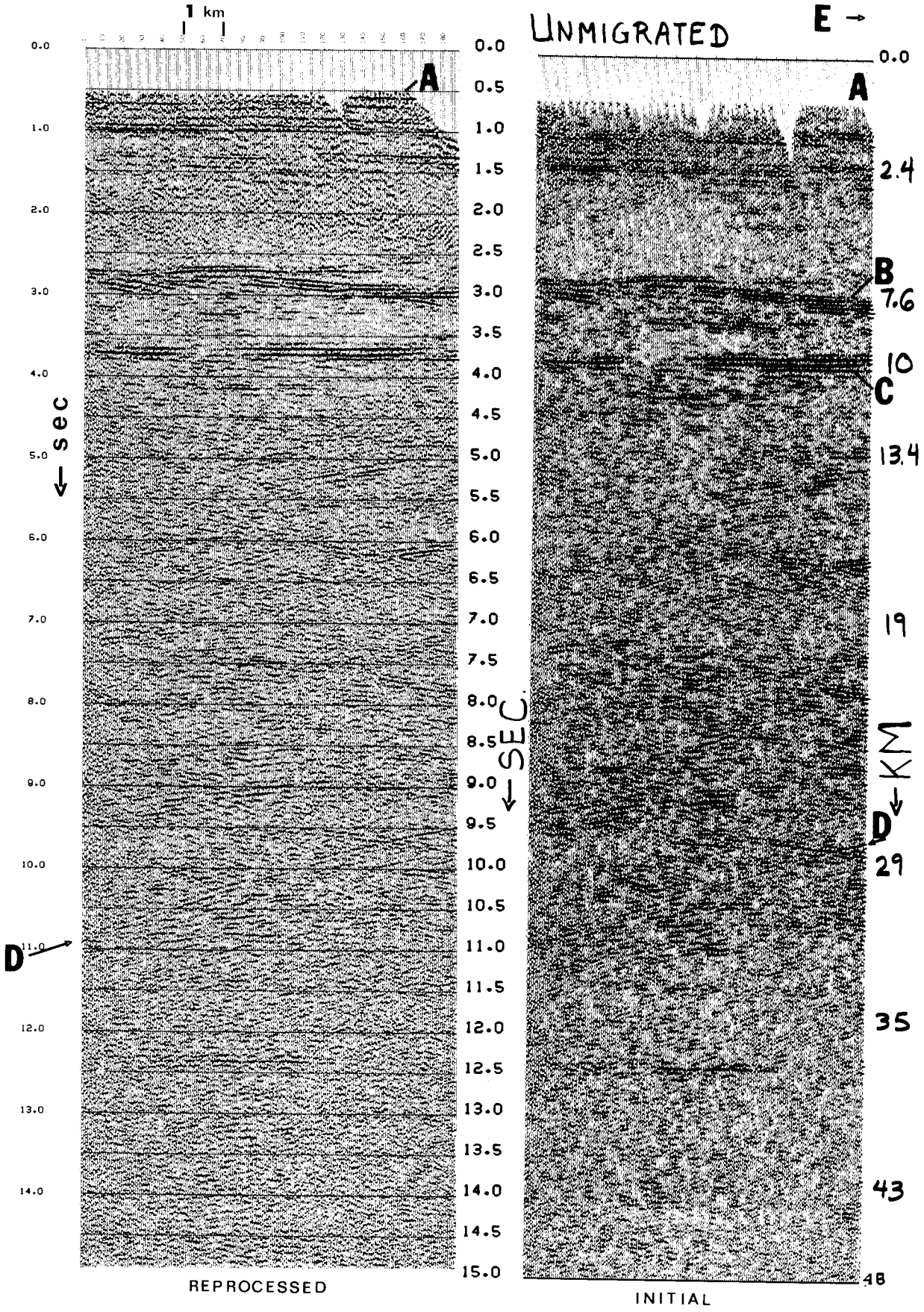
1 km
A
D
sec
0.0
1.0
2.0
3.0
4.0
5.0
6.0
7.0
8.0
9.0
10.0
11.0
12.0
13.0
14.0
0.0
0.5
1.0
1.5
2.0
2.5
3.0
3.5
4.0
4.5
5.0
5.5
6.0
6.5
7.0
7.5
8.0
8.5
9.0
9.5
10.0
10.5
11.0
11.5
12.0
12.5
13.0
13.5
14.0
14.5
15.0
SEC
REPROCESSED
UNMIGRATED
E →
A
B
C
D
0.0
2.4
7.6
10
13.4
19
29
35
43
48
KM
INITIAL

FIG. 2.5.

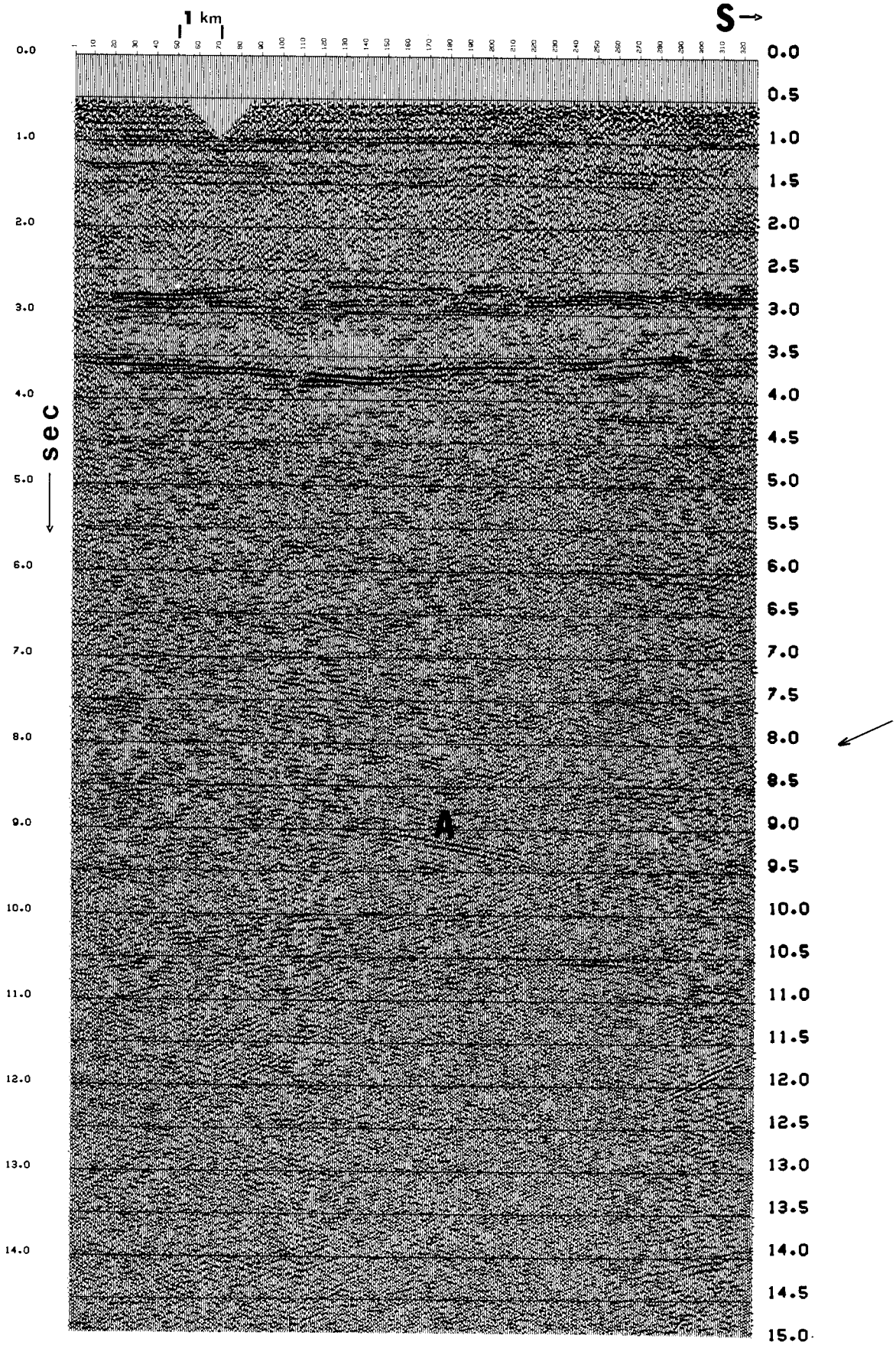
1 km
S→
sec
0.0
1.0
2.0
3.0
4.0
5.0
6.0
7.0
8.0
9.0
10.0
11.0
12.0
13.0
14.0
0.0
0.5
1.0
1.5
2.0
2.5
3.0
3.5
4.0
4.5
5.0
5.5
6.0
6.5
7.0
7.5
8.0
8.5
9.0
9.5
10.0
10.5
11.0
11.5
12.0
12.5
13.0
13.5
14.0
14.5
15.0

FIG. 2.6.

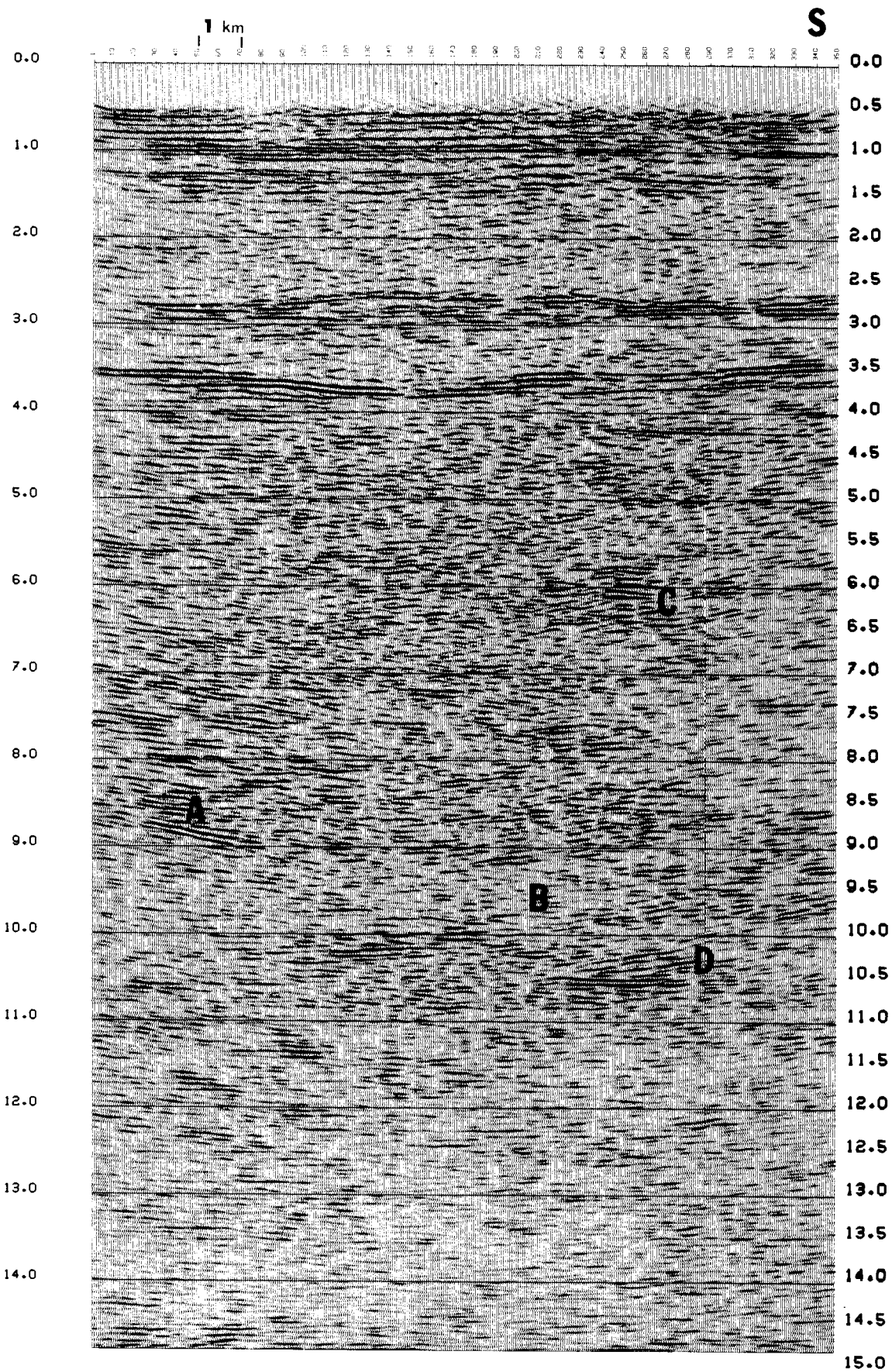
1 km
S
A
B
C
D
0.0
1.0
2.0
3.0
4.0
5.0
6.0
7.0
8.0
9.0
10.0
11.0
12.0
13.0
14.0
0.0
0.5
1.0
1.5
2.0
2.5
3.0
3.5
4.0
4.5
5.0
5.5
6.0
6.5
7.0
7.5
8.0
8.5
9.0
9.5
10.0
10.5
11.0
11.5
12.0
12.5
13.0
13.5
14.0
14.5
15.0

FIG. 2.7.

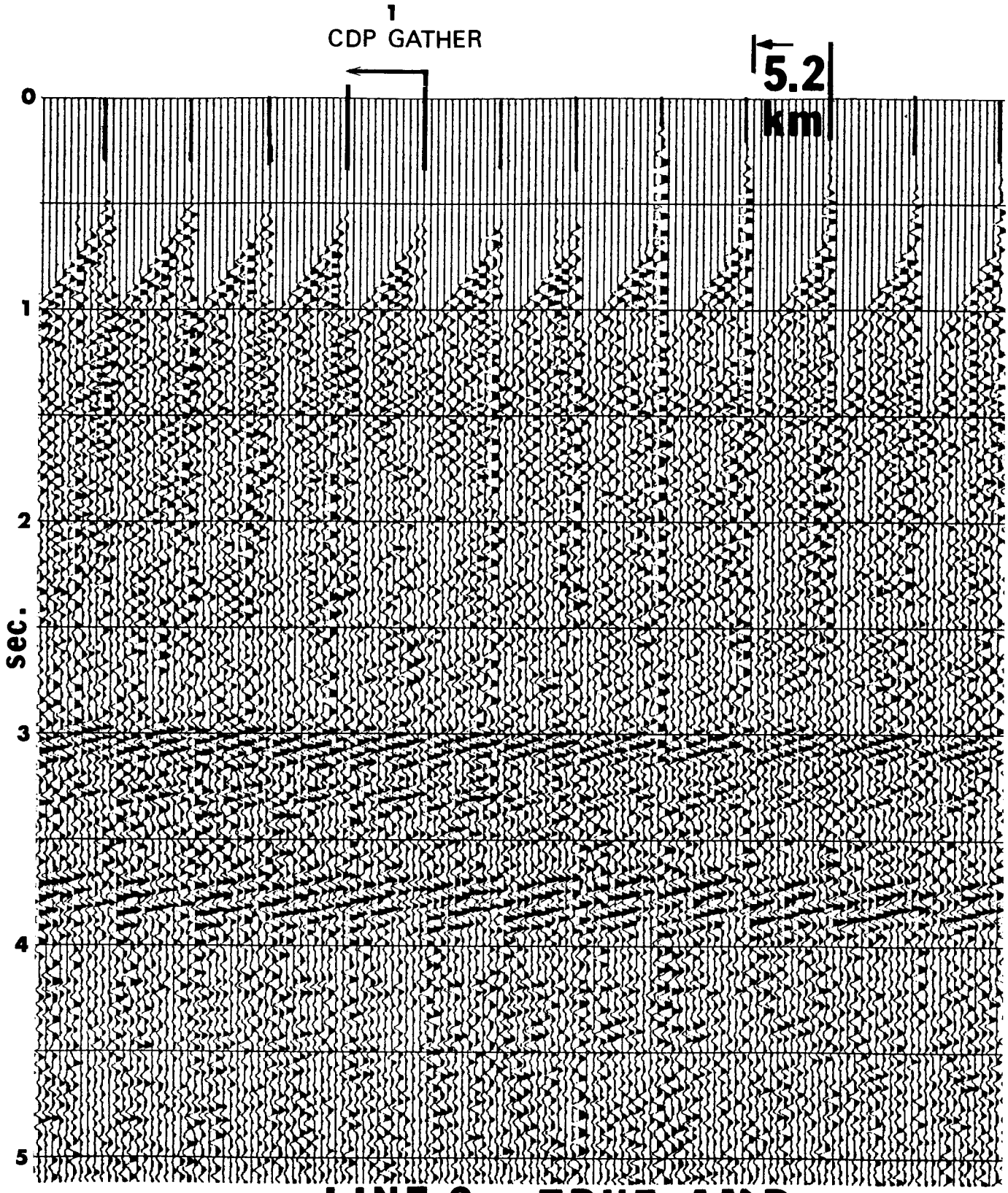

FIG. 2.8A.

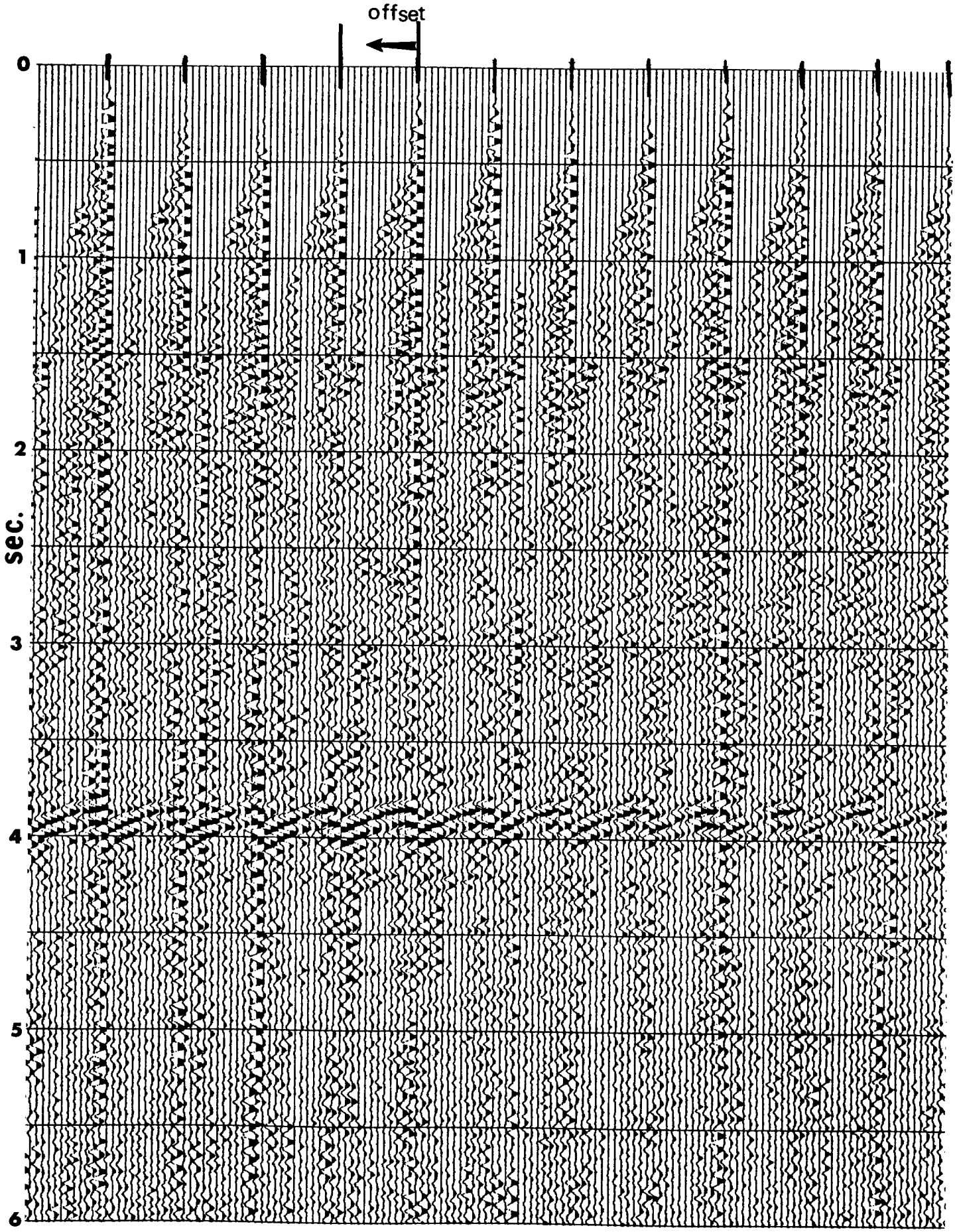

LINE 1 - TRUE AMP.

FIG. 2.8B.

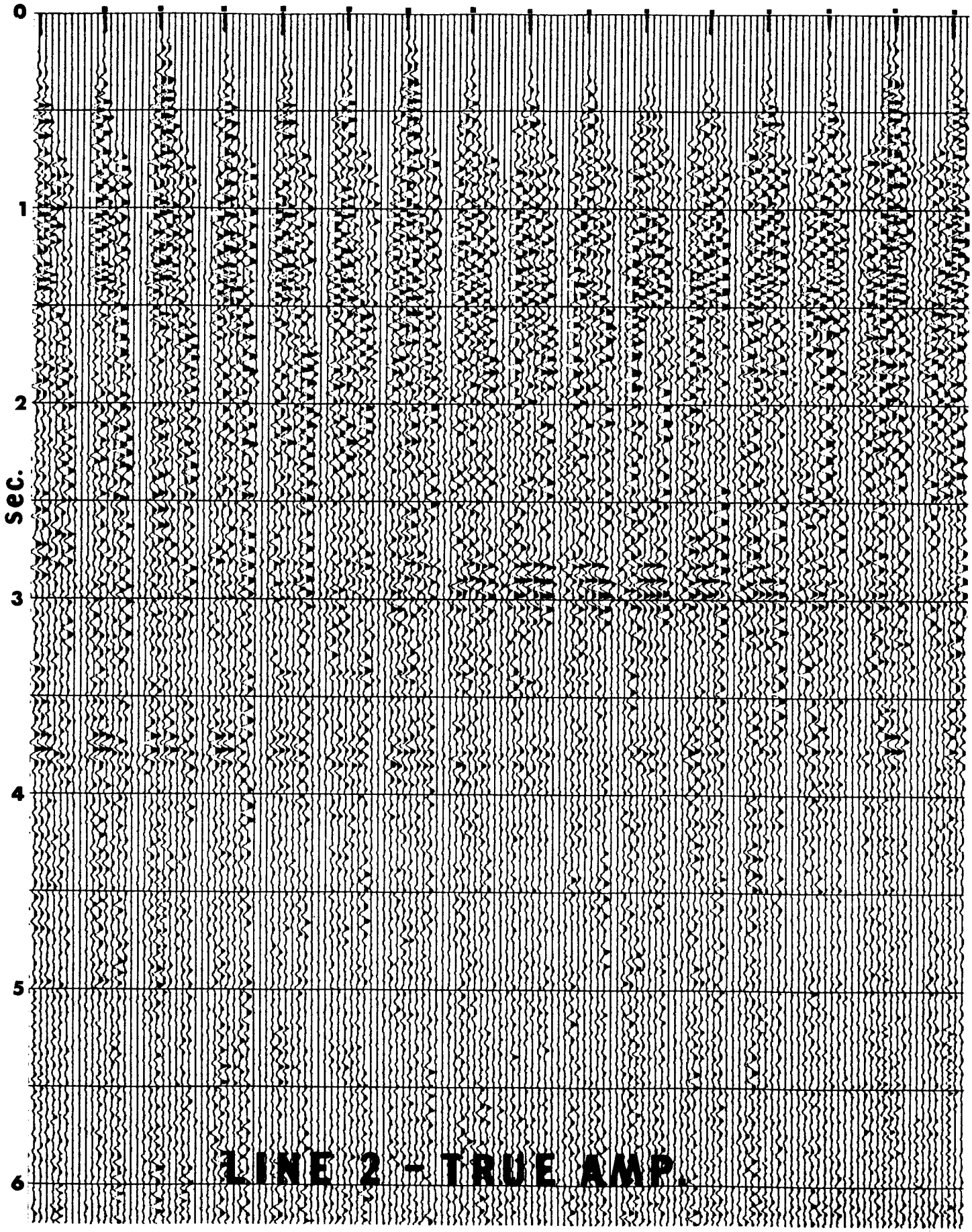

FIG. 2.8C.

As expected, the effect of migration was to enhance reflector continuity and thereby emphasize the layered yet heterogeneous nature of the crust at this location. Diffractions are collapsed (see arrow, Figure 2.6, Figure 2.7) and dipping energy is correctly placed in time and space within the limits of a two-dimensional dataset and algorithm (*e.g.*, event A, Figures 2.6 and 2.7).

The well data locates the top of basement at 1.415 sec. Layered reflectors between 1.415 sec and ~1.6 sec (Figures 2.2-2.4) lie above a seismically transparent zone between ~1.6 and 2.8 sec. At ~2.8 and ~3.8 sec, high-amplitude continuous reflectors are seen. Their thickness and arrival times vary across the sections. On the original processing (A, Figures 2.2-2.4), usually 4 cycles (or legs) per event are seen. The continuity and amplitude of the 2.8 and 3.8 sec high-amplitude events rival and exceed (respectively) that of the sedimentary reflectors. Between those two reflectors are several discontinuous reflectors ~1 km in lateral extent.

From 3.8 to 11 sec, short (0.5-1.0 km) discontinuous reflections have various dips (C,D, Figures 2.2-2.4). Some regions within this part of the crust appear almost seismically transparent (B, Figure 2.7), but not as transparent as between 1.6 and 2.8 sec. Other zones have a high density of reflectors (C, Figure 2.7). Divergent and convergent dip segments are seen throughout the migrated lines from 4 to 11 sec. A striking example of "dip splaying" is seen on line 1 at 10.5 sec (D, Figure 2.6). This character of the seismic response of the crust is seen clearly on migrated sections, and obscured on the unmigrated data. The seismic features will be interpreted later.

At 11 sec, there is a substantial reduction in energy. Oliver *et al.*, 1976, also noted the change on the unmigrated time section. Below 11 sec, there is a further decrease in the number of reflectors, and in their amplitude. Migration greatly enhanced a 12.4 sec reflector on line 2 (Figure 2.3) that is easily seen on the unmigrated data but without such a marked amplitude contrast.

RELEVANT GEOLOGICAL AND GEOPHYSICAL DATA

Interpretation requires a working knowledge of the relevant geologic and geophysical data. Presented first is a summary of the regional geologic setting: the distribution of rhyolite, granite, and gabbro known from basement core samples from wells; and the basement lithologies and spatial relationships seen in outcrop and well data in the Wichita Mountains, southwest Oklahoma. Secondly, geologic hypotheses concerning epizonal batholiths, heat sources, and bimodal (mafic-silicic) volcanism are examined in relation to the local data for Hardeman Cty. and the regional geology in northern Texas/southwestern Oklahoma. Thirdly, previous regional seismic/velocity work, including reflection, refraction, and well data, has yielded valuable information. The interval velocities in the Hardeman dataset further constrain the interpretation.

Regional Geologic Setting - Hardeman Cty., Tx.

Geologists have abundant well information concerning basement in most of Texas and southwestern Oklahoma. Muehlberger *et al.* (1967) and Flawn (1956) utilized hundreds of core sample analyses for mapping basement lithology beneath the cover of younger rocks (Figures 2.9 - 2.11). The oldest rocks in this region are the eastern New Mexico 1570-1650 m.y. sequence of gneiss, schist, and quartzite with granitic, granodioritic and quartz-dioritic intrusions. These rocks are labeled GN in Figure 2.9. Possibly somewhat younger are granite and associated granite-gneiss, schist, quartzite, metarhyolite, and amphibolite (TOR, Figure 2.9). This region has been interpreted as consisting of a 1570-1650 m.y. or older basement on which a cycle of sedimentation, metamorphism, and intrusion was superimposed (Muehlberger *et al.*, 1967).

The Chaves granitic terrane (CH), to the southwest of Hardeman Cty., is also dated at ~1350 m.y. and consists largely of granite, granodiorite, and gneiss of similar composition. Eighty percent of the samples studied were granitic in composition. Most of the

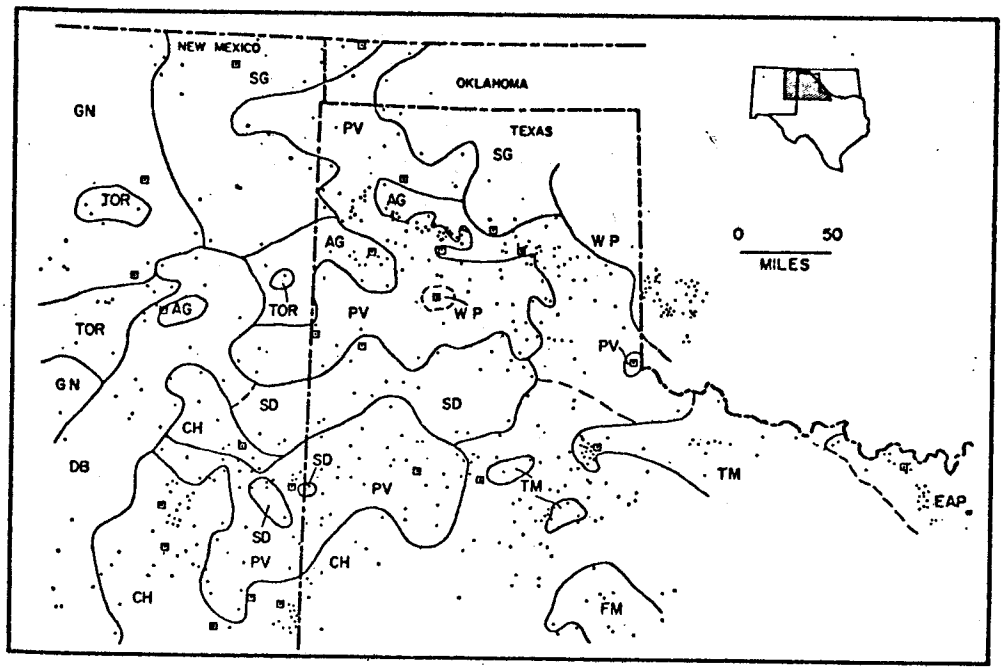

—Geologic map of Precambrian rocks of Texas Panhandle and eastern New Mexico; includes Cambrian igneous rocks of Wichita province (WP). Dots = samples studied; squares = isotopic ages reported in Muehlberger *et al.* (1966); GN = older gneiss and granite; TOR = older metasedimentary and meta-igneous rocks; CH = Chaves granitic terrane; PV = Panhandle volcanic terrane; SD = Swisher diabasic terrane; AG = Amarillo granite terrane; SG = Sierra Grande granite terrane; DB = De Baca terrane; TM = Tillman metasedimentary group; FM = Fisher metasedimentary terrane; EAP = Eastern Arbuckle province.

FIG. 2.9. Geologic map of basement rocks of the Texas Panhandle and eastern New Mexico (from Muehlberger *et al.*, 1967).

metasedimentary rocks belonged to the green-schist facies, although well cores also sampled amphibolite and diorite gneiss. Figure 2.9 shows that these rocks are nearer the Hardeman lines than the TOR metasediments. Diabase is also encountered in this terrane. "Diabase, found in wells as dikes in granitic rocks or as the only basement rock drilled, is considered to be younger than the granitic and metamorphic rocks because it is unmetamorphosed (Muehlberger *et al.*, 1967).

A third terrane recognized as part of the older basement in Texas is the Sierra Grande Granite terrane (SG). Dated at 1270 m.y., it is a nonfoliated medium- to coarse-grained biotite granite to granodiorite.

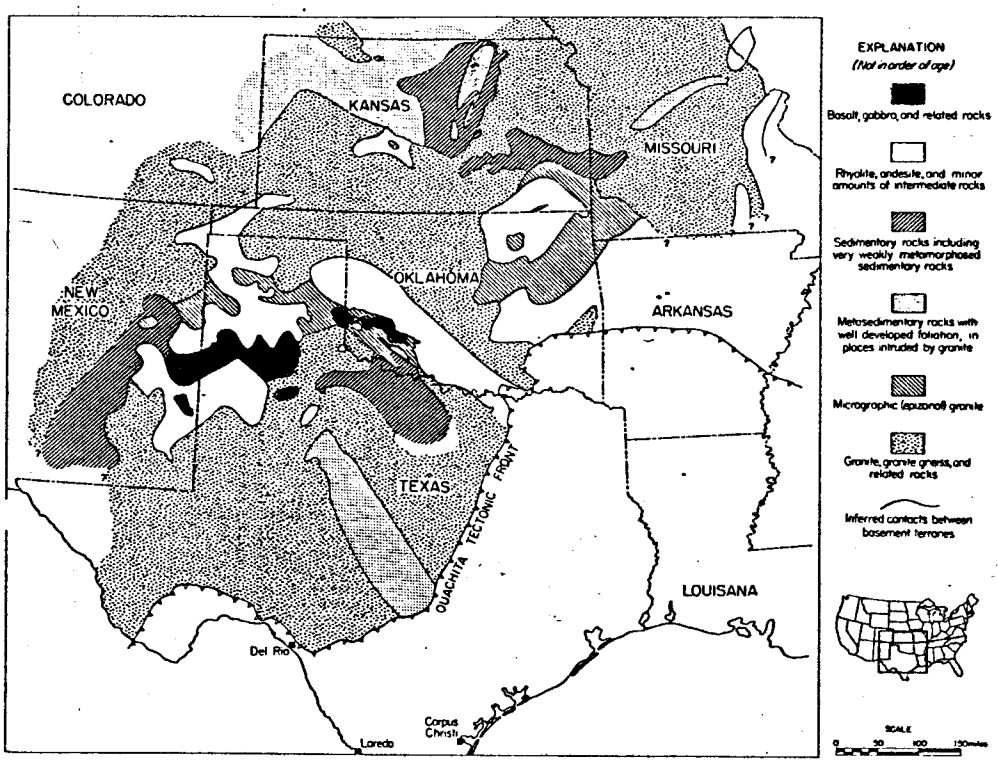

Distribution of lithologic types within the largely concealed Precambrian basement of south-central United States. According to HAM, DENISON, and MERRITT (1964), Wichita Mountains rocks are 500 Myr to 550 Myr old and consequently are Cambrian. Modified from BAYLEY and MUEHLBERGER (in preparation).

FIG. 2.10. Distribution of lithologic types within the largely concealed Precambrian basement (from Flawn and Muehlberger, 1970).

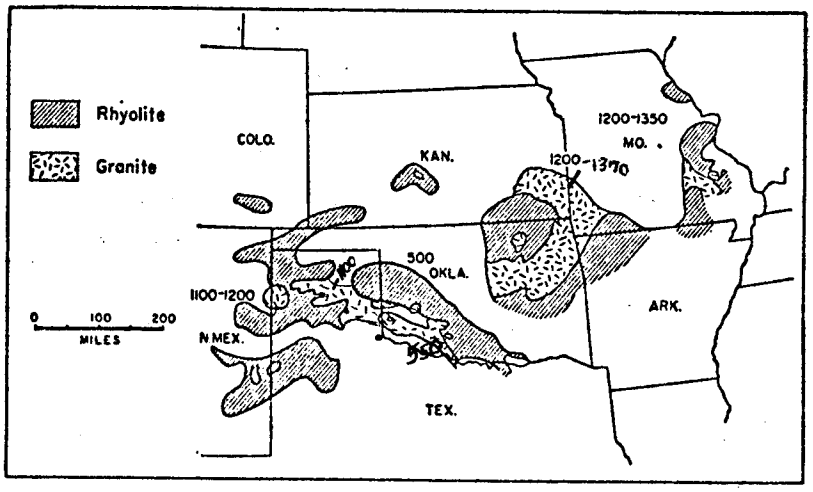

Distribution of rhyolite and associated epizonal granite, south-central United States. Isotopic ages in millions of years of each segment indicated (modified from Muehlberger *et al.*, 1966). Sources of data: Ham *et al.*, 1964 (southern Oklahoma); Denison, 1966 (northeastern Oklahoma and vicinity); Edwards, 1966 (Colorado); Scott, unpub. (Central Kansas); Flawn, 1956 (Texas and New Mexico, modified by present writers); Denison, unpub. (Missouri).

FIG. 2.11. Distribution of rhyolite and associated epizonal granite, southcentral U.S. (modified from Muehlberger *et al.*, 1967).

The Panhandle volcanic terrane (PV) is believed to overlie all the units described above. It consists of extensive rhyolite porphyrys and tuffs with smaller amounts of rhyodacite, trachyandesite, and andesite (Figures 2.9,2.10). The extrusive character of most of the rhyolite has been established unequivocally by petrographic studies (Muehlberger *et al.*, 1967). These rhyolites are dated between 1100 and 1250 m.y. (Flawn and Muehlberger, 1970). One 500 m.y. date may indicate that some parts of this large rhyolitic terrane in northern Texas may be contemporaneous with the Cambrian rhyolite of the Wichita Mtns., in southern Oklahoma. In Potter County, 209 km NW of the Hardeman County lines, 1.15 km of volcanics containing 80 m diabase was drilled without reaching basement. "Several cores from widely spaced wells showed only low dips on flowage structures, indicating that this thick, layered rhyolite is nearly horizontal" (Muehlberger *et al.*, 1967).

The Amarillo granite terrane (AG), shown on Figure 2.9 as underlying most of Hardeman County, is believed to be an epizonal plutonic equivalent of the Panhandle volcanics (Flawn and Muehlberger, 1970). Figure 2.10 shows Hardeman County underlain by granite, granite gneiss, and related rocks. This granite terrane, 1100-1200 m.y. old, comprises granites and granodiorites, with considerably more mafic granitic rocks found in the eastern Panhandle (near Hardeman) than in the western extent of this terrane. In the central Panhandle, granite intruded rhyolite, and in northeast Potter County (241 km to the NW), a granite sill above metarhyolite were drilled.

The Swisher diabasic or gabbroic terrane (SD) is a stratiform mass of gabbro and diabase extending for ~250 km across New Mexico and Texas (Figure 2.9, 2.10). Well data suggests that the gabbroic rocks intruded rhyolites and late Precambrian metasedimentary rocks (carbonates, argillaceous or arkosic siltstones). A K-Ar date on pyroxene from one gabbro sample yielded 1200 m.y. (Flawn and Muehlberger, 1970), but pyroxenes often contain excess argon, leading to spuriously old ages (Hyndman, 1972). Roth (1960) cited diabase cutting Pennsylvanian fossiliferous limestone in the Humble No. 1 Howard Ranch well, Briscoe County, indicating that at least some of the diabase is post-Pennsylvanian. "The regional distribution of these rocks and their

association with the sedimentary rocks of demonstrable Precambrian age in eastern New Mexico suggests that most of the basalt and gabbro in the Texas Panhandle is Precambrian" (Flawn and Muehlberger, 1970).

The Wichita igneous province (Flawn, 1956) consists of rhyolite, epizonal granite, and gabbro petrographically similar to the Wichita Mtns. rocks (as discussed later, Figures 2.9, 2.10). There are both Precambrian and Cambrian dates on these rocks indicating that (1) there are at least two and maybe more episodes of intrusive/extrusive igneous activity in northern Texas, and (2) that the Precambrian Panhandle volcanics apparently have mafic rocks associated with them in time and space, as seen in northern (WP) and north-central Texas (Swisher diabase terrane).

The Tillman metasedimentary group (TM) (Flawn, 1956) is typically a poorly sorted meta-graywacke, argillite, quartzite, and bedded chert of biotite metamorphic grade (Flawn, 1956). At least 4.5 km thick, it is interpreted to be a marine eugeosynclinal deposit of possible Early Cambrian (Precambrian?) age. It appears to lie on a 1150-1350 m.y. basement. As it is near the Hardeman lines, it may have been seismically sampled.

Regional distribution of epizonal granites and rhyolite. If all of south-central U.S. is examined (Figure 2.11), we find that basement beneath 155,000 sq km (60,000 sq miles) of the south-central U.S. is rhyolite and epizonal granite. From ~1370 m.y. to ~1100 m.y. ago, silicic magma was emplaced at shallow levels and erupted from northern Ohio, through Missouri, Kansas, Oklahoma, into the Texas Panhandle. These igneous events overlap in time and space; the original extent of the volcanic piles is unknown. The Precambrian volcanic areas become younger southwestward, with the exception of the middle Cambrian (500 m.y.) Wichita Province, SW Oklahoma. Where these extrusive rocks are present, the approximate top of Precambrian crust is preserved. Seismic experiments over a "preserved section" of continental crust would be of interest to compare with sections where the intermediate crust is exposed due to erosion.

Wichita Mountains, SW Oklahoma, outcrops. At least 1.37 km of 525 m.y. rhyolite and at least 0.2 - 0.5 km of granite overlie two apparently different gabbroic intrusions (pers. comm., B. Powell, and C. Gilbert). The older gabbro is a layered intrusion, comparable in type though not in size, to the Bushveld complex. A younger biotite gabbro intrudes the layered gabbro. R.E. Denison and B. Powell (pers. comm.) suggest that these mafic rocks were uplifted and eroded prior to the arrival of the comagmatic rhyolites and granites, although no erosional contact is seen in the field. Later diabase dikes and possibly sills cut both the gabbroic and granitic rocks.

Subsurface data, SW Oklahoman basement. The following is a summary of SW Oklahoman basement from Flawn and Muehlberger (1970). A crystalline basement was formed 1350-1450 m.y.a. in south-central U.S., probably by a major geosynclinal cycle or cycles. Epizonal granites intruded and rhyolite erupted onto this basement (Figure 2.11). There are slightly younger epizonal silicic rocks in Missouri (1200-1350 m.y.) and still a younger sequence in the Texas Panhandle (1100-1200 m.y.). The final event in the basement in this region is the basalt-gabbro-rhyolite-granite sequence in southern Oklahoma of Early to Middle Cambrian age.

Association of Silicic and Mafic Magmas in the Upper Crust

Epizonal granitic batholiths are generally tabular, and capped by their own ejecta according to Hamilton and Myers (1967). Gabbroic underplating of silicic magma chambers has been proposed based upon the time-space eruptive relations seen in the field for several caldera cycles (Bailey ***et al.***, 1976; Hildreth, 1979). Long-lived magma chambers require either great burial depth or continued input of heat to prevent solidification and ensure the longevity evinced by eruptive histories of silicic volcanic centers (Lachenbruch ***et al.***, 1976). The most effective transfer fluid to supply heat to the upper crust is molten basalt (Shaw ***et al.***, 1968). Thus it would not be surprising to find seismic evidence for gabbro in association with epizonal batholiths. The reflection coefficient of the granite/gabbro interface, 0.14, would

yield an excellent, clearly visible reflection.

Basaltic magma, originating in the mantle by partial melting of peridotite, can rise into the crust through dikes if the stress conditions are favorable (least principal stress horizontal, as in a tectonic drift). Yoder (1976) described the mantle process as "magmafracting," analogous to hydrofracting in commercial oil well stimulation or in the measurement of ***in situ*** stress. The upward flux of basaltic magma can cause partial melting of the lower to middle crust. If intrusion of mafic melts and consequent crustal heating is sustained, basaltic and silicic melts would eventually rise into the upper crust. Silicic magmas could melt some of the already hot country rock during their ascent (Eichelberger and Gooley, 1977). At shallow depths a granitic melt may tend to spread out into a thin lens at the level of its own density, dependent upon viscosity, heat loss, and resistance of the enclosing rocks. Some granitic magmas intrude and crystallize directly beneath their own slightly older ejecta (Hamilton and Myers, 1967). However, a silicic magma chamber would trap rising mafic magmas under it such that mafic magma would erupt only ***around the periphery*** of the silicic magma chamber (Hildreth, 1979). The "shadow zone" for basaltic eruptions observed on the earth's surface in an area of silicic volcanism shows the horizontal limit of the silicic magma chamber. Unable to rise through the silicic magma chamber, the mafic magma may spread beneath the silicic chamber. Termed gabbroic (or basaltic) underplating, this will create a granite-gabbro pair. Cyclic magmatic events could produce multiple pairing of granite-gabbro. When the silicic magma crystallizes sufficiently to allow brittle fracture, mafic melt will once again erupt in the former shadow-zone.

Regional and Local Velocity Information

Seismic refraction lines in Oklahoma. The results of refraction surveys in southern Oklahoma are shown in Figures 2.12 and 2.13, taken from Tryggvason and Qualls (1967) and Mitchell and Landisman (1970). The applicable data in these figures come from the Anadarko

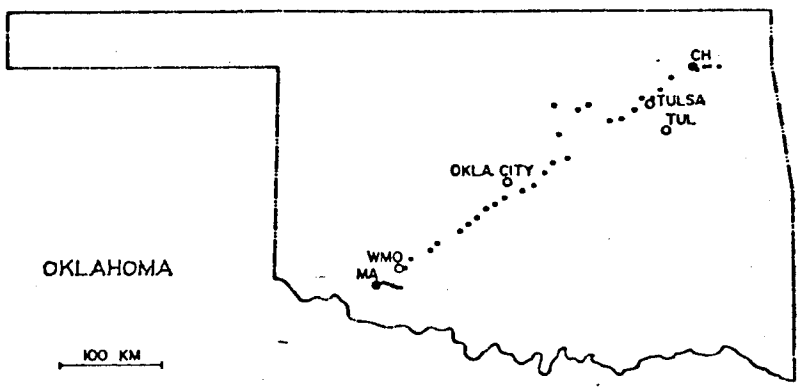

Location of the refraction profile in Oklahoma 1964. The two permanent seismological observatories in Oklahoma, Wichita Mountains Observatory (WMO) and Leonard Observatory (TUL) are shown. Shot points, double circles; recording sites, small circles.
CH = Chelsea, MA = Manitou.

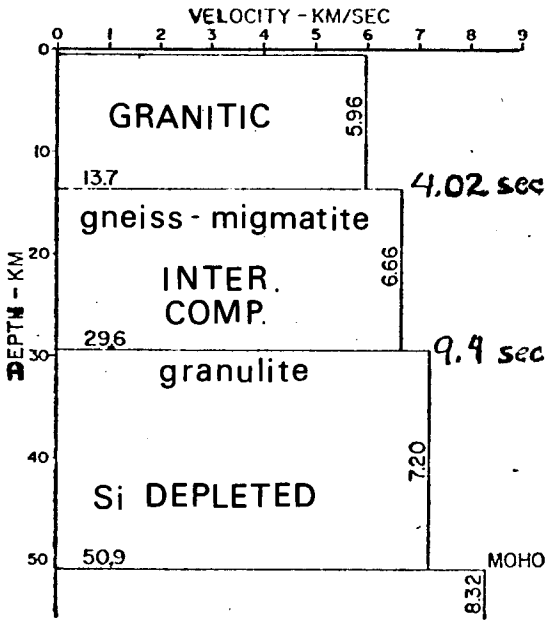

Oklahoma earth model assuming homogeneous horizontal layers.

FIG. 2.12. Results of Tryggvason and Qualls (1967) seismic refraction work in so. Okla. Compare with Figure 2.13

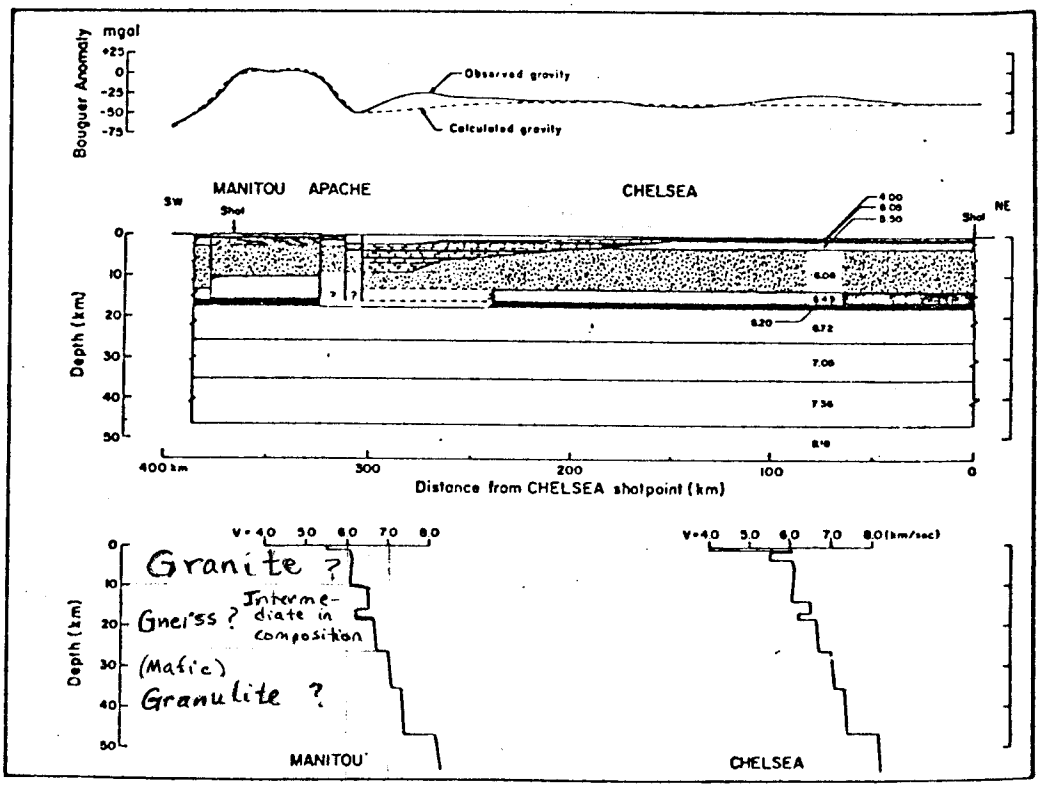

(Top) Theoretical and observed gravity anomaly values along the profile. (Middle) Crustal model with average velocity values indicated for each layer. Dotted lines indicate uncertain positions of boundaries. The limestone symbol only implies fast sediments and does not necessarily indicate limestone or flat-lying beds. Vertical exaggeration: X2. (Bottom) Velocity-depth curves near the Chelsea and Manitou shot points.

FIG. 2.13. Results of Mitchell and Landisman's (1970) refraction work in so. Okla. Compare with Figure 2.12.

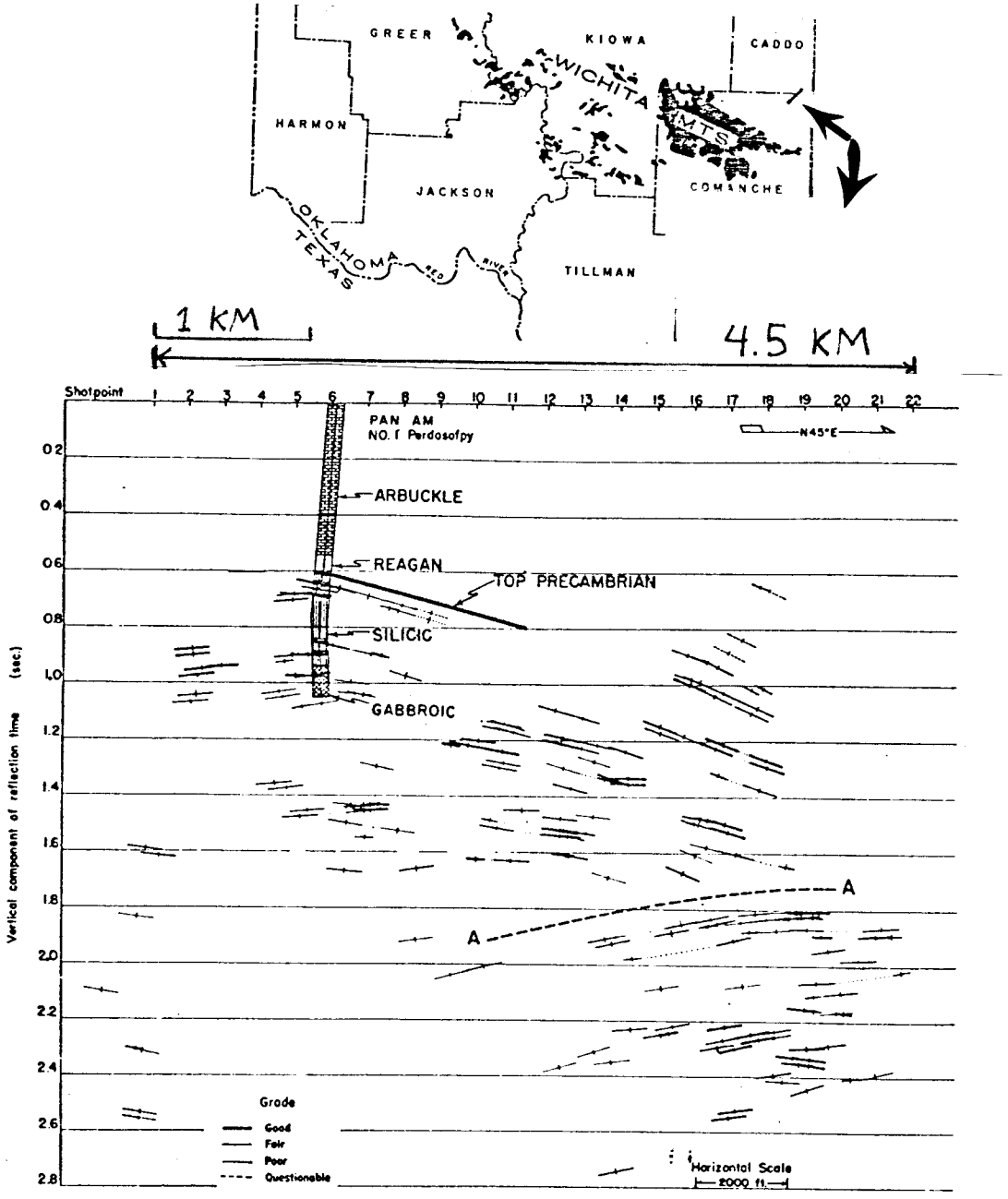

Seismic cross-section in terms of migrated time. The Pan American No. 1 Perdasofpy is shown in its projected position, and its log is transcribed to time using velocity measured in the well. About 4,000 ft of pre-Cambrian igneous section was penetrated by the well. The line A-A marks an abrupt change of seismic dip that precludes multiple reflections.

FIG. 2.14. Migrated (by hand) seismic section from south-western Okla. 1.5:1 H.E. Note top of basement at ~.6-.8 sec, and the strong intra-basement reflectors to ~2.4 sec (~7.2 km) (from Widdess and Taylor, 1959).

Basin region, ~100 km NE of the Hardeman seismic lines (Figure 2.14). Both datasets suggest there may be gross velocity divisions in the crust, as given below.

DEPTH	VELOCITY
~1-12 km (.3-4 s)	~6.0 km/s
~12-28 km (4-9~s)	~6.5 km/s
~28-46 km (9-15 s)	~7.2 km/s

These velocities guided the choice of intermediate and deep-crust migration velocities.

Seismic reflection data in Oklahoma. Widdess and Taylor (1959) reported persistent (over several km) and good-quality reflectors within the Precambrian basement, in southwestern Oklahoma 135 km northeast of the Hardeman County lines (Figure 2.14). A well (the Pan Am. No. 1 Perdasofpy) 0.7 km southeast of the seismic line revealed that the reflections from ~.6-1.0 sec (1.8-3 km) came from extrusive silicic rocks; the reflections at ~1.0 sec (and probably most of those below) came from gabbroic rocks. The data from this well ends at ~1.05 sec, while primary reflections continue to at least ~2.6 sec (~7.5 km). The seismic reflections are interpreted as alternating layers of silicic and mafic rocks (Widdess and Taylor). A thrust fault, probably associated with the Wichita Mountain uplift, is suggested by a marked change in dips in the basement.

Elsewhere in northern Texas and southwestern Okla., seismic reflections having the layered appearance of sedimentary rocks have been drilled for oil, only to find either rhyolitic flows, or sheetlike bodies of diorite and/or diabase intruding granite (as at the Phillips No. 1 Matoy, Bryan Cty., Okla.; Ham ***et al.***, 1964). These deceptive reflections indicate widespread igneous basement rocks which (seismically) resemble sedimentary rocks.

Velocities in igneous rocks, from well data, SW Oklahoma. The sonic logs from three wells which penetrated ~40 feet of Wichita Province basement (~500 m.y. old, younger than the Hardeman basement, see

Figure 2.9) recorded rhyolite velocities of 4.3 - 5.5 km/s. Granite velocities averaged about 5.8 km/s. Eastern Arbuckle cataclastic granites had velocities between 5.5 and 5.8 km/s. These granites are about the same age as the Hardeman basement rocks, but their slower velocities may be due to their proximity to and participation in major faulting and the consequent fracturing. Faster Hardeman basement seismic interval velocities may also be partially due to a more intermediate bulk composition.

Seismic interval velocity information from the Hardeman data. The stacking velocity (if no dip is present) approximates the RMS velocity. The stacking velocity as a function of time is determined by measuring the normal moveout (hyperbola curvature) on unstacked data. Dix's equation yields interval velocities from RMS velocities in areas of no dip. The interval velocities, when used with laboratory data on rock velocities, determine possible lithologies for the rocks at depth.

The original processing velocities, the Schilt and Long (Cornell University) reprocessed velocities, and the seismic interval velocities from these stacking velocities are given in Appendix 2. The velocities (to 1.42 sec) from the Pan Am. No. 1 Bestwall Gypsum sonic and seismic velocity survey, the migration (rms) velocities, their interval velocities, and the average interval velocities from the reprocessed data are given in Table 1. The migration velocities came from the well data, the best agreement among the Cornell stacking velocity functions, and the refraction data. Overall, the reprocessed velocity functions are a significantly better match with the well velocities. Better stacking velocities have improved the appearance of the stacked sections, both above and below 1.42 seconds.

Velocities and densities from laboratory data. Laboratory measurements of velocity and density link measured earth velocities (reflection and refraction) with possible lithologies. A plot of velocities and densities for rocks of interest in the continental crust is shown in Figure 2.15. The velocities from 1.4 - 4 sec in Table 1 can be compared with Figure 2.15 to estimate the bulk composition of that interval. The interval velocities indicate silicic – to – intermediate

TABLE 1: MIGRATION VELOCITIES

Int. Vel. (km/s)	Time (sec)	Rms. Vel. (km/s)	
	0.0	1.83	From Pan. Am. Bestwall Gypsum sonic & seis. vel. survey
2.95			
	.345	2.95	
4.31			
	.485	3.4	
3.71			
	.595	3.46	
3.67			
	.735	3.5	
4.06			
	.981	3.65	
4.31			
	1.247	3.8	
5.42			
	1.315	3.9	
5.12			
	1.417	4.0	
5.53			From best fit of stacking vel. fcns. (re-processed vels.)
	1.65	4.25	
6.12			
	2.8	5.1	
6.49			
	3.8	5.5	
6.66			
	5.0	5.8	
6.69			
	7.35	6.1	From refraction vels.
6.83			
	11.0	6.35	
7.24			
	15.0	6.6	

Average Interval Velocities From Reprocessed Stacking Vel. Fcns. (in Appendix 2)

(sec)	(km/s)
1.4	
	5.68
1.6	
	5.87
2.8	
	6.32
3.8	
	6.3
~5.0	

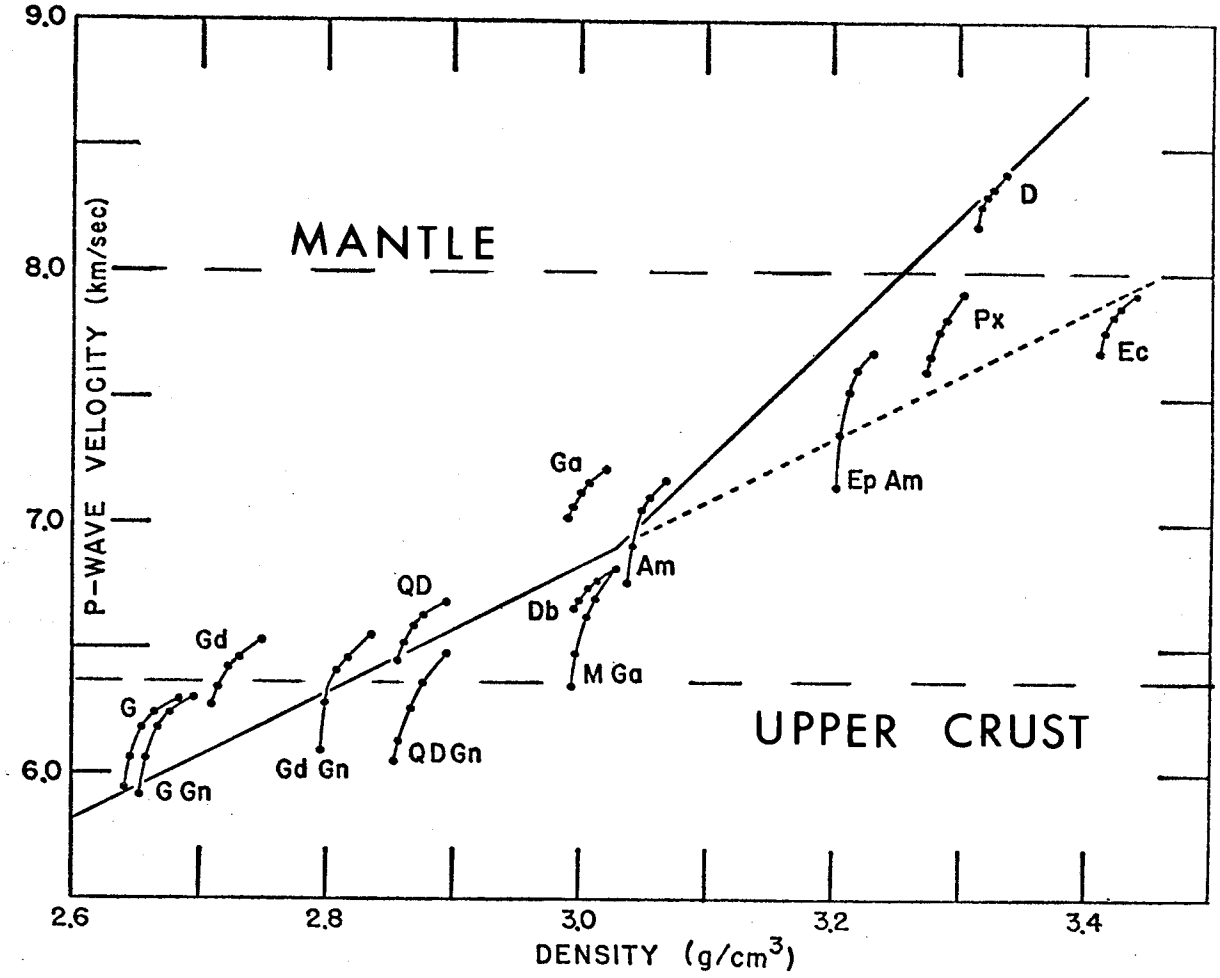

Experimental data (*15, 16*) on P-wave velocities as a function of confining pressure for selected igneous and metamorphic rocks. From bottom to top, data points for each rock type correspond to pressures of 1, 2, 4, 6, and 10 kilobars. The solid curve based on these data was used to estimate densities of the rocks composing the seismic columns from their velocities. Approximate lithostatic pressures corresponding to the tops of the seismic "layers" are plotted opposite the appropriate layer velocities at left. *G*, Granite from (i) Westerly, Rhode Island, (ii) Chelmsford, Massachusetts, and (iii) Barre, Vermont, and quartz monzonite from Porterville, California (*15*); *GGn*, gneiss 1 and gneiss 2 (*16*) from Berkshire Highlands; *Gd*, granodiorite from Butte, Montana (*15*); *GdGn*, gneiss 3 and gneiss 4 (*16*) from Berkshire Highlands; *QD*, quartz diorite from San Luis Rey, California, and Dedham, Massachusetts (*15*); *QDGn*, gneiss 5 from Berkshire Highlands (*16*); *Ga*, gabbro from Mellon, Wisconsin, and French Creek, Pennsylvania, and norite from Pretoria (*15*); *Db*, diabase from (i) Holyoke, Massachusetts, (ii) Centerville, Virginia, (iii) Sudbury, Ontario, and (iv) Frederick, Maryland (*15*); *MGa*, metagabbro from Hodges Mafic Complex (*16*); *Am*, amphibolite 1 and amphibolite 2 (*16*) from Mount Tom; *EpAm*, epidote amphibolite 1 and epidote amphibolite 2 (*16*) from Hodges Mafic Complex; *Px*, pyroxenite from Sonoma County, California, and bronzitite from Stillwater Complex and Bushveld Complex (*15*); *D*, dunite from Twin Sisters Peaks, Washington (*15*); *Ec*, eclogite from Healdsburg, California, and Kimberly (*15*).

FIG. 2.15. Rock velocities and densities, determined from laboratory data, from Bateman and Eaton (1967), and Birch (1960).

rocks (such as granite to granodiorite) in this interval, rather than mafic rocks. Below 4 sec, the interval velocities do not yield reliable numbers. The error bars on the seismic interval velocities are discussed in the next section.

Analysis of Velocity Resolution

Seismic data is sampled in time, and so the normal-moveout correction can be at best measured and applied to the nearest sample. Discretized moveout corrections yield discretized stacking velocities and discretized interval velocities. While few geophysicists agonize over the normal moveout to the nearest sample, this restriction affects the conclusions possible about the rocks at depth. The analysis of stacking velocity discrimination uses the given velocity function, the normal moveout equation, the sample rate (.008 sec), and the farthest available offset as a function of time (the muting function) to determine the resolution possible. When the moveout of the longest live offset is varied by ± one sample, the velocity so indicated will be decreased/increased. The lower and higher velocities so determined constitute the resolution in stacking velocity afforded by the dataset. The limit of resolution in stacking velocity determines the resolution possible in interval velocity calculation. Further discussion of this method is in the Appendix.

Of the three ***initial-processing*** stacking velocity functions, the two most widely used indicated velocities appropriate for silicic rocks (~5.7 km/s) (Curve A, Figure 2.16) from 1.3-3.8 sec. Only the southern 3 km of line 1 (7% of the data) seemed to indicate the faster velocity function, and thus mafic rocks (6.9-7.2 km/s) below 1.3 sec to 3.8 sec (Curve B, Figure 2.16). However, the velocity discrimination afforded at the end of the line is very poor, and so these higher velocities are not reliable. The two silicic velocity functions are distinguishable from the mafic velocity function.

The best ***reprocessed*** stacking velocity function, which was used to migrate the data (Table 3), is Curve C, Figure 2.16. It agrees with the velocity function for silicic rocks from 1.3-2.8 sec. Therefore, the

section from 1.3-2.8 sec is interpreted as silicic rocks. From 2.8-4.4 sec, the velocity is intermediate between and distinguishable from the other two functions. The improved velocities suggest silicic-intermediate rocks from 2.8-3.8 sec, but unfortunately, a difference of one sample in the normal-moveout correction at ~3.8 sec will change the interval velocity from 6.4 km/s (silicic to intermediate rock types) to 7.1 km/s (gabbro velocity). A change in inferred rocktype will also change the geologic interpretation. However, on both initial and secondary processing, the lower velocity function indicating silicic to intermediate rocks was consistently picked on the velocity analyses. It is here tentatively accepted as indicating that silicic (to intermediate) rocks exist between 2.8-3.8 sec.

INTERPRETATION OF DATA

The top of basement (1.4 sec) is known from well data to be Precambrian rhyolite. The reflections from ~1.42 - 1.6 sec (~0.5 km thick) are interpreted to be layered rhyolite flows and tuff (Figure 2.17). These reflections may be generated by porosity within the rhyolite. The seismic response of layered rhyolite in northern Texas and Oklahoma has been documented (Widdess and Taylor, 1959; Ham ***et al.***, 1964). These flat-lying reflectors are often mistaken for (and drilled as) sedimentary rocks. The seismic interval velocity, 5.75 km/s, from 1.4-1.6 sec on Hardeman line 1 is close to the well velocity of Cambrian rhyolite (~5.5 km/s) in Oklahoma.

We interpret the seismically transparent zone (~1.6-2.8 sec, ~3.6 km thick) to be the zone wherein rhyolite becomes seismically indistinguishable from granite. The loss of porosity from the rhyolite due to sufficient pressure and temperature will cause extrusive silicics to seismically resemble their intrusive equivalents. The interval velocities indicate a silicic composition for the interval 1.3-3.8 sec. This interval is interpreted as a tabular pluton, intruding and overlain by its own ejecta.

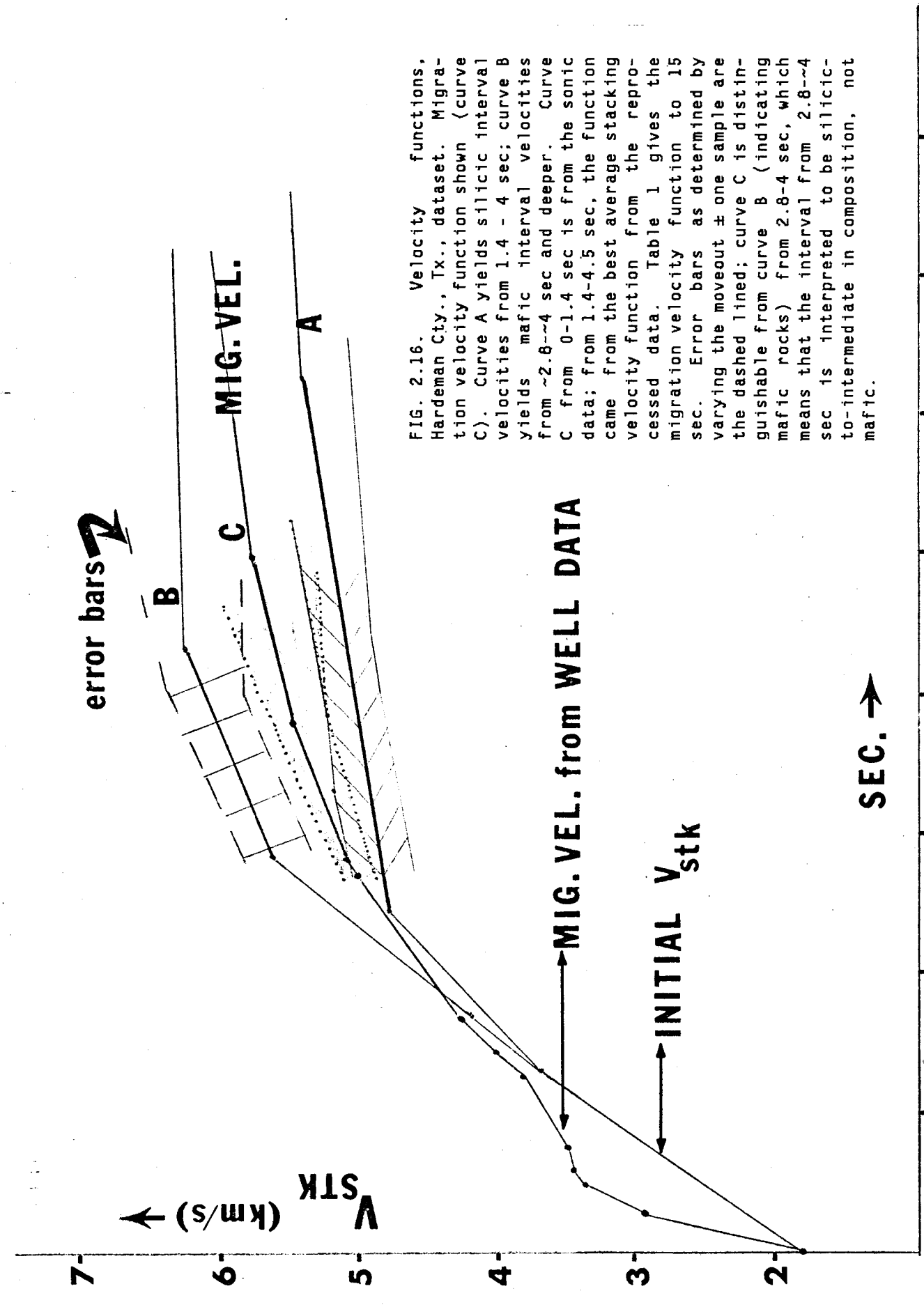

FIG. 2.16. Velocity functions, Hardeman Cty., Tx., dataset. Migration velocity function shown (curve C). Curve A yields silicic interval velocities from 1.4 - 4 sec; curve B yields mafic interval velocities from ~2.8-~4 sec and deeper. Curve C from 0-1.4 sec is from the sonic data; from 1.4-4.5 sec, the function came from the best average stacking velocity function from the reprocessed data. Table 1 gives the migration velocity function to 15 sec. Error bars as determined by varying the moveout ± one sample are the dashed lined; curve C is distinguishable from curve B (indicating mafic rocks) from 2.8-4 sec, which means that the interval from 2.8-~4 sec is interpreted to be silicic-to-intermediate in composition, not mafic.

FIG. 2.17. Migrated line 1, with the interpretation of the seismic data. 17 km lateral extent is displayed. To convert from sec to km, multiply by 3 (which assumes an average crustal velocity of 6 km/s). The data is interpreted as a silicic complex ~7.5 km thick, overlain by ~2.9 km Paleozoic sediments. The top ~.6 km of the complex is porous tuff and flows, grading downward into ~3.5 km of comagmatic granite. The lower 3.2 km of the complex, between the two high-amplitude reflectors, is interpreted as granitic to granodioritic rocks. Highly reflective mafic sills (~2.8 sec, and ~3.8 sec) are interpreted to indicate two pulses of bimodal plutonism. The tabular silicic pluton is underplayed by gabbroic rocks, rather than passing imperceptibly into migmatite.

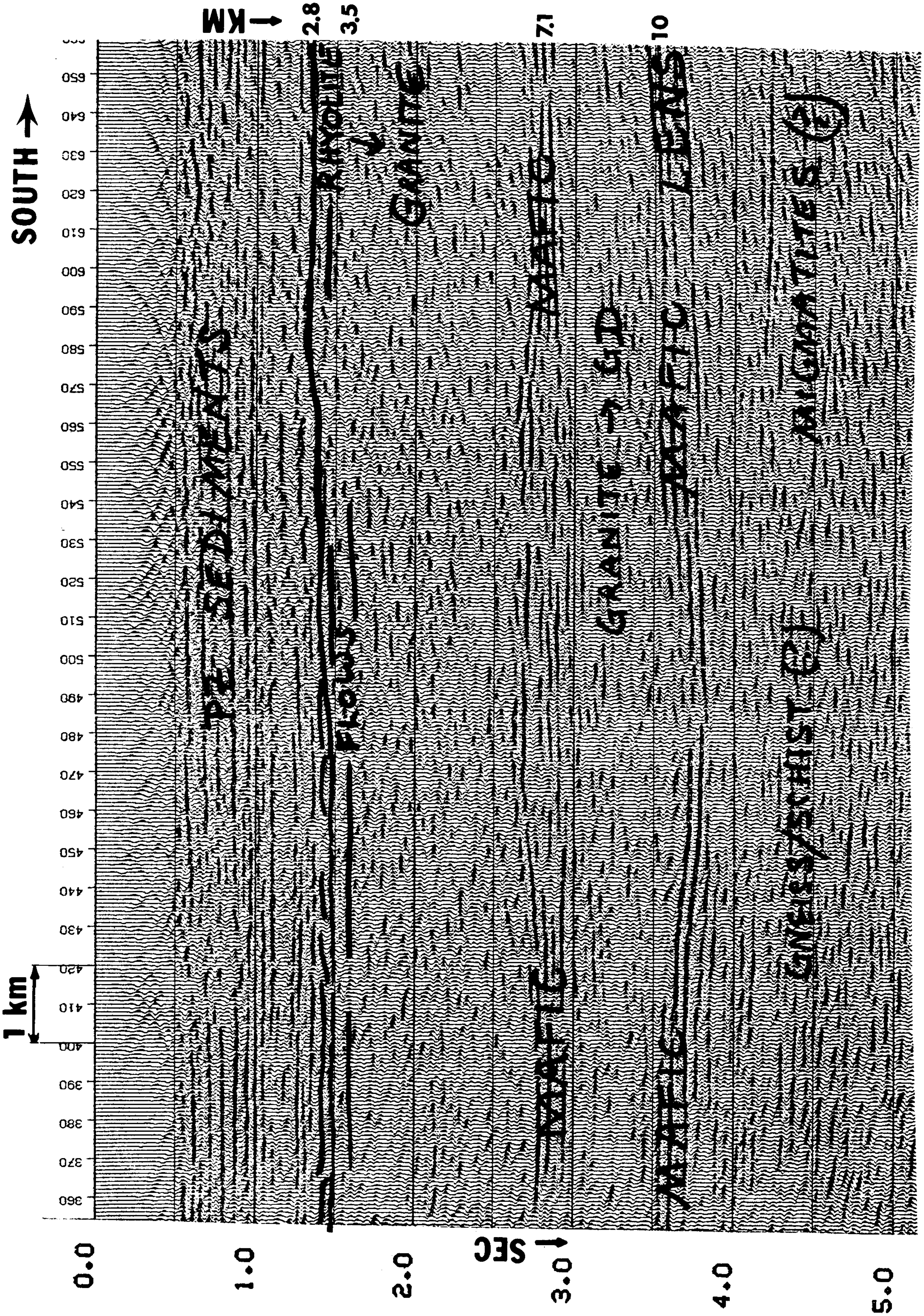
SOUTH →
1 km
KM →
2.8
3.5
7.1
10
SEC
0.0
1.0
2.0
3.0
4.0
5.0
360
370
380
390
400
410
420
430
440
460
470
480
490
500
510
520
530
540
550
560
570
580
590
600
610
620
630
640
650
PZ SEDIMENTS
RHYOLITE FLOWS
RHYOLITE → GRANITE
MAFIC
MAFIC
GRANITE → GD
MAFIC LENS
MAFIC
GNEISS/SCHIST (?)
MIGMATITES (?)

FIG. 2.17.

The remarkably high amplitude of the two reflectors (~2.8 and ~3.8 sec) near the middle and at the base of the pluton demands a substantial change in seismic impedance. Mafic rocks with a density of 3.0 g/cc and a velocity of ~7.0-7.2 km/s are obvious candidates. The thickness of the sills varies but averages about 800 m thick. The variability in amplitude as seen on the true-amplitude gathers (Figure 2.5) can be explained by variable thicknesses (100-1000 m thick), since the thickness of a reflective layer can influence the amplitude of the reflection. The average higher reflectivity of the lower mafic lens, as seen on the true-amplitude gathers, suggests that this is a more consistently thick lens, wherein destructive interference between the top and bottom reflections is minimal. The higher reflectivity (spatially averaged) of the lower lens may indicate the major change from igneous body to underlying country rocks. Since the interval velocities from 2.8-3.8 sec indicate silicic-to-intermediate compositions, it is possible that this pluton is "zoned" to granodioritic rocks in the lower half of the pluton. High- level magma chambers are known to be compositionally zoned to more mafic compositions at deeper levels through the study of voluminous ash-flow sheets (Lipman, 1966; Hildreth, 1979). Alternatively, Eichelberger and Gooley (1977) have proposed that "hybridization" of silicic and mafic magmas could result if there is an infusion of fresh basaltic magma into the base of a silicic magma chamber, after the latter has begun to cool in the upper crust. The seismic data may be revealing the result of such an infusion. The seismic data display what one would expect if such a hybridization did occur.

The heat in two 800 m thick lenses of mafic magma emplaced under 7 km of silicic magma would allow 0.2-0.4 m.y. to elapse before the silicic batholith would solidify. This estimate assumes conductive heat losses, no losses by hydrothermal convection, and includes the latent heat of crystallization. Lachenbruch *et al.* (1976) used 0.1 m.y. as "the time constant for the propagation of a temperature disturbance by conduction" through a roof 5 km or so thick above a magma chamber. The ~0.3 m.y. estimate is a short time span, compared to that of the regional silicic volcanism (~100-150 m.y.).

A single, thick gabbro body (~2.8 to ~3.8 sec, ~3.5 km thick) with strong reflectors at its top and bottom is an alternative but unlikely possibility because the interval velocities in that zone indicate a silicic-to-intermediate composition. The geologic observation made earlier that the Amarillo granite terrane tends to be more mafic to the east (Hardeman Cty.) is corroborated by these interval velocities which, high for granite, approach those of granodiorite.

Obviously, the seismic data do not give time relationships; perhaps one or both of the high-amplitude reflectors represents a mafic intrusion not associated with the silicic pluton. By analogy, in the Wichita Mountains, the epizonal granite intrusion was cut by later diabase/basalt dikes. The dike-shape of the mafic intrusions indicates that the silicic body had cooled enough to support brittle fracture.

At Hardeman County, we prefer the interpretation of a lengthy magmatic episode, which is known by the geologic record, with at least two pulses of contemporaneous granite and gabbro. Our interpretation explains the subhorizontal nature of the two reflectors, the high reflection coefficient, and integrates the data with the known regional abundance of epizonal granite, rhyolite, and gabbro. The interval velocities between 2.8 - 3.8 sec indicating the intermediate (chemical composition) rocks and the several discontinuous reflectors in that interval are also explained, using either Eichelberger and Gooley's (1977) hybridization model or the zonation model (Lipman, 1966; Hildreth, 1979).

Below 3.8 sec, the seismic character of short dip segments may indicate subhorizontal, discontinuous, compositional layers with thicknesses of the order of the seismic wavelengths (300 m or more), possibly within a section of migmatites, schists, or gneisses. The widespread Tillman metasediments could be part of this section; it is dominantly graywacke, but also contains siltstone, shale, sandstone, arkose, and bedded chert metamorphosed to biotite grade. Another candidate for the sub-batholith material is the Red River mobile belt rocks consisting of meta-graywacke and meta-arkose. Metasediments, migmatites, and amphibolites may comprise the crust here to ~11 sec (33 km).

Oliver *et al.* (1976) suggested that seismically transparent crustal zones may be plutons (homogeneous rocks) and that layered zones may be schist/gneiss. However, if these zones can be thus identified, migrated sections with reasonable (30-45-degree) dip coverage to deep-crustal depths must be used (see Chapter 1).

A complication in the interpretation of migrated deep crustal data is the effect of interference or "tuning" among layers with very small impedance contrasts. Mayer (1979) reported that in his marine high-resolution (4 kHz) work, very low reflection coefficients (10^{-3} to 10^{-5}) created seismic reflections suggesting high reflection coefficients. In his investigation and sampling of the upper 10 m of the sedimentary column, Mayer found that the reflectors seen on the seismic profile did not correlate with discrete geologic horizons but rather were caused by interference effects between many small layers. If his work is extended to deep-crustal seismic profiling, which is also band-limited (6-25 Hz), the implication is that deep crustal reflectors (*e.g.* at 12.5 sec, Figure 2.3) may be zones of fortuitously spaced flat layers of rocks with very small reflection coefficients which through interference yield a "high"-amplitude reflection. Also, by implication, seismically "transparent" zones need not be homogeneous igneous bodies ("plutons") but could be zones of layered, gneissic, or generally inhomogeneous rocks, which at the given frequency band ***appear*** transparent.

At ~11 sec occurs a change in seismic character. Migrated sections are expected to display a gradual increase in event continuity with time, a gradual decrease of amplitude with time, and a decrease in dip angles with time, because of limited cable length, the shortness of the lines, and the length of recording time. However, neither ***all*** the event continuity nor the ***abrupt*** decrease of amplitude at 11 sec can be explained simply by the migration of a line limited in extent. One possibility is that a granulite (anhydrous) region may exist below ~11 sec.

The high-amplitude event at 12.5 sec, line 2 (Figure 2.7), is also seen on the cross line, line 1, but with a smaller amplitude. This reflection is not thought to be from the Moho. While the amplitude of the reflector indicates a marked velocity-density change at that

interface, refraction work in southern Oklahoma (100 km to the NE) indicates that the Moho is ~50.9 km deep (Tryggvason and Qualls, 1967). The VIBROSEIS field records were recorrelated by Oliver and Kaufman (1977) using a shorter sweep to extend the record time from 15 sec to 18.5 sec They conclude that the events at 15.5 sec, about 50 km deep, are probably reflections from the Moho.

Geologic exposures of the lower continental crust in NW Spain (den Tex and Vogel, 1962) and in Venezuela (Morgan, 1970) provide physical models for the deep, high-amplitude, subhorizontal reflector. A massive hornblende-bearing eclogite layer up to 500 m thick and 4 km long occurs within banded granulite in NW Spain. In Puerto Cabello, Venezuela, eclogite and associated mafic rocks occur as conformable sheets and lenses (~200 m thick, 5-200 km long) within country rocks of epidote-amphibolite facies. Thus the high-amplitude event at 12.5 sec is interpreted as a lens of eclogite ~500 m thick, ~2 km long. An alternate interpretation, as discussed above, is interference or "tuning" among many fortuitously spaced layers of small impedance contrasts.

DISCUSSION

The regional abundance of epizonal granites, associated with rhyolites of the same age and chemistry, supports our interpretation. Moreover, the Swisher gabbroic terrane 50 km to the west, covering 1.6 x 10^4 sq km in Texas and New Mexico, and the voluminous mafic intrusions in and around the Wichita Mts. 50 km to the northeast, prove that there has been also abundant mafic magmatic activity in this region. Comagmatic granite and overlying rhyolite, underlain by two different gabbros, outcrop in the Wichita Mtns. This close spatial occurrence of tabular bimodal igneous rocks serves as a possible model for the older occurrence in Hardeman County.

We suggest that rising mafic magmas, generated in the mantle, intruded the lower continental crust, heated and partially melted it, enriching the lower crust in mafic components and depleting it in

silicic components by generating ascending silicic magmas. The refraction velocities support this interpretation of a noticeably silica-depleted lower crust. The silicic magmas (heated by mafic magma below) rose in the crust. The silicic plutons could have been capped by country rock or by their own slightly older volcanic ejecta. Rising basaltic magma would sill out beneath the silicic magma chamber because of the latter's lower density (Eichelberger, 1978). The absorption of heat from the mafic magmas along with new additions of melt from depth may have sustained the eruptions over the length of time observed in south-central U.S.

An unknown amount of silicic extrusives was removed by erosion from the top of the pluton. Elsewhere in Texas, 1.8 km of rhyolite was drilled without reaching the base of the rhyolite; if there were once 2 km of extrusive rocks at Hardeman County overlying the Amarillo granite terrane, then the original thickness of the silicic complex may have approached 9 km. Using Muehlberger *et al.'s* (1967) basement map (Figure 2.9), the extent of the Amarillo granite terrane is ~320 km in length, and between 15-110 km in width. An average thickness of 7-9 km would make this somewhat eroded epizonal batholith thinner than laterally extensive (Hamilton and Myers, 1967).

Based on models of batholithic emplacement and bimodal volcanism, it is conceivable that the spatially related silicic and mafic activity in northern Texas are at least thermally and possibly genetically related as described here. Similar relations might also hold in southwestern Oklahoma where the silicic rocks are Cambrian and the mafic rocks are not yet reliably dated. We suggest that the bimodal igneous activity seen from northern Texas through southwestern Oklahoma indicates incipient rifting. The widespread shallow granitic/rhyolitic terranes of Precambrian age in south-central U.S. may be the result of major partial melting of the lower continental crust ~1370-1100 m.y. ago.

Other Seismic Data from Areas of Granite Intrusions

Seismic reflection data collected by T. McEvilly across the San Andreas (Figure 2.18) was migrated by Laura Gagnon using a 45-degree depth migration (Kjartansson, 1979) at Stanford. There are high-amplitude, approximately horizontal reflectors with a layered appearance at 7-10 km (2.5-3.5 sec) in the west part of the line (on the Pacific plate) where Gabilan granite outcrops at the surface. These reflectors, not seen underlying the deformed Franciscan sedimentary rocks on the North American side, are interpreted as layers underneath the granite pluton. While these reflections could be from thrust faults associated with an old subduction zone, they could also be from a mafic sill or lens underneath the granite.

A 27-km reflection seismic profile was shot across Black Rock Desert and Haulapai Flat, Nevada (Callaway, 1978). This is a Cenozoic interior basin between bedrock mountain ranges. The profile shows three prominent reflecting horizons (at 0.5 sec, 1.0 sec, and 3.0 sec) (Figure 2.19). The interval from 0.1-.5 sec (.28 km depth) was interpreted to be unconsolidated clays with an interval velocity of 1.1 km/s; the interval from .5-1.0 sec (.28-.8 km), volcanic and sedimentary rocks with an interval velocity of 2.2 km/s; and the interval from 1.0-3.0 sec (.8-6.1 km), the Mesozoic granodiorite exposed to the west (less than 10 km away) in the Granite Range and to the east in Trego Mtn. The seismic interval velocity from ~1 to 3 sec is ~5.4 km/s, but interval velocity resolution at this depth is poor (±.5 km/s). We interpret the strong subhorizontal reflections at 3.0 sec to be from the base of the ~5.3 km thick granite. The reflectors may represent mafic lenses (gabbroic underplating) or the upper part of a thicker mafic body.

Strong, subhorizontal reflections are seen under granitic plutons in California, Nevada, and Texas, although ages and tectonic setting differ. A long-standing question has been the nature of sub-batholithic rocks. A gradual downward transition to migmatites has often been suggested but the strong reflectors present on the Hardeman dataset rule out this possibility. In at least some cases the sub-batholithic rocks may be predominantly mafic rocks, and possibly layered.

FIG. 2.18A. A true-amplitude unmigrated seismic time section across the San Andreas (traces 125-150) showing layered reflectors (left sides, 2.75-3.5 sec) beneath the Gabilan granite, Ca. Note diffraction tail to left of the high-amplitude event (0.75 sec, tr. 107).

FIG. 2.18B. The migrated depth section: the time delays caused by the velocity decrease associated with the fault zone are removed. The layered reflections (7-10 km) under the granite may be a gabbroic underplating, similar to that observed at Hardeman Cty., Tx. Note focused high-amplitude event (1.1 km depth, tr. 108).

FIG. 2.19. An AGC'd unmigrated seismic time section in the Basin and Range province, Nev., showing strong, layered reflectors (~3.0 sec). These reflectors underlie an interpreted granodioritic body (1.0-3.0 sec, 0.8-6.1 km depth), which is exposed in outcrop in the adjacent block-faulted mountain ranges. These reflectors may be further seismic indication of gabbro underplating an intermediate magma chamber.

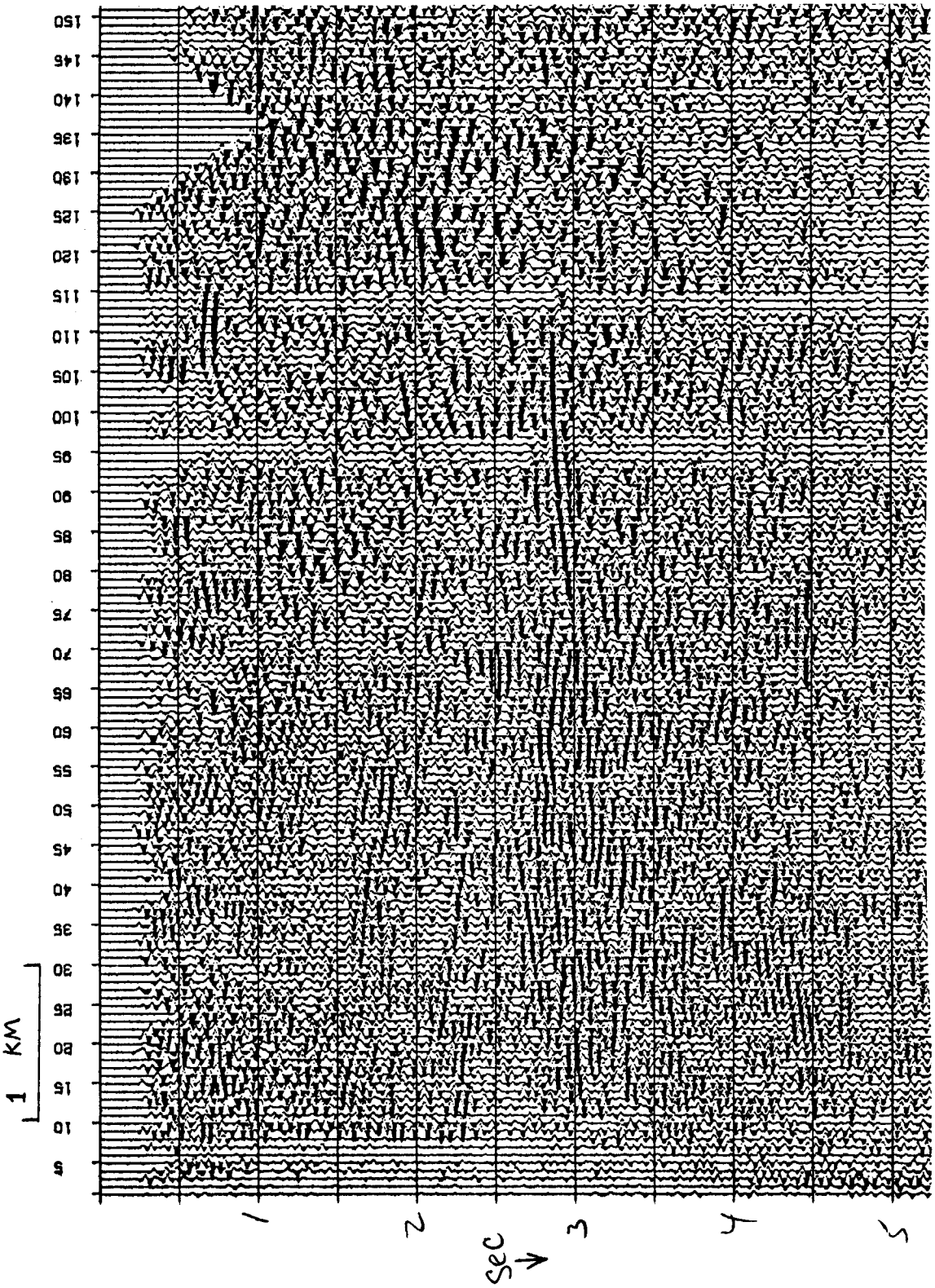

FIG. 2.18A.

MIGRATED DEPTH SECTION

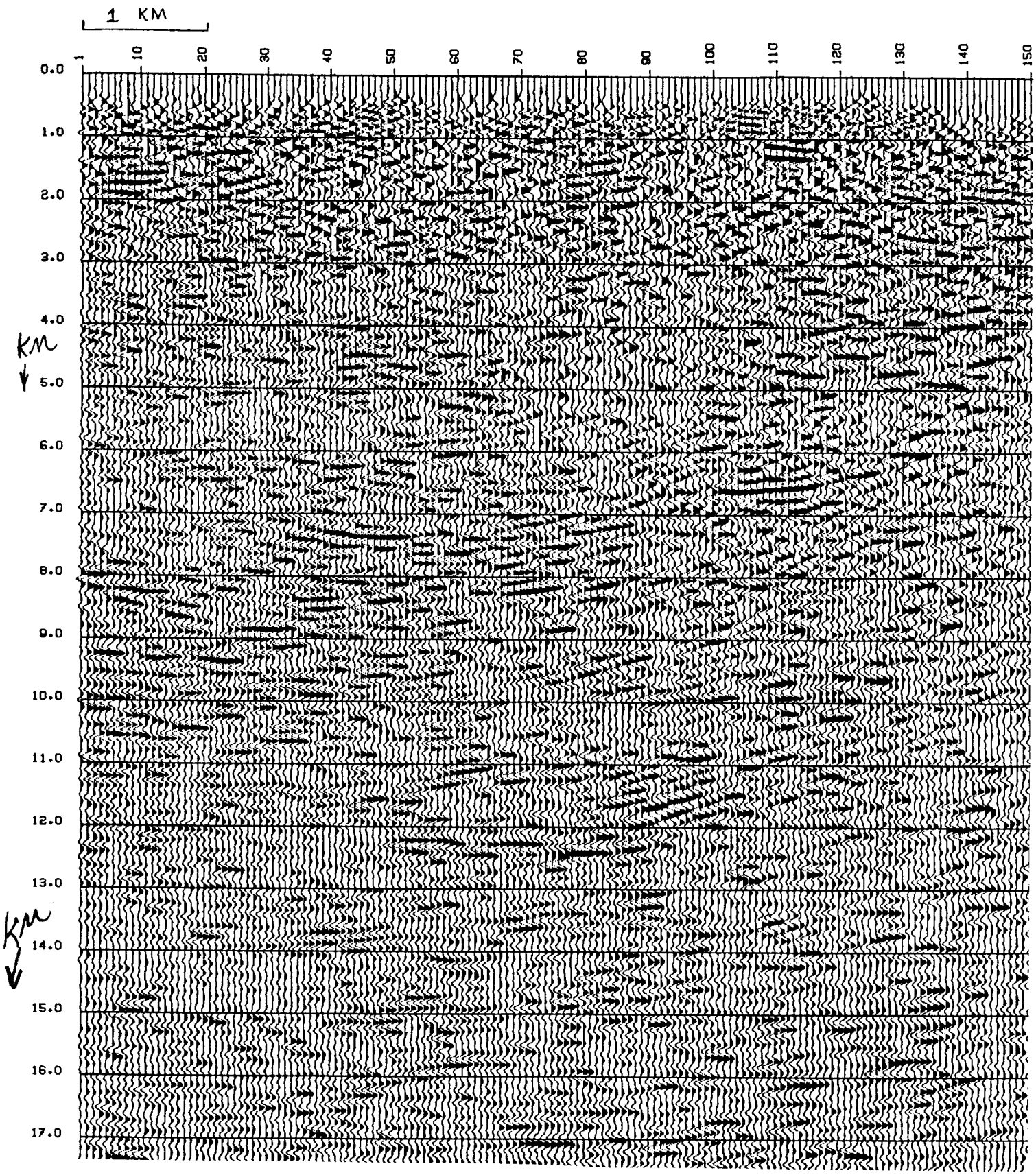

FIG. 2.18B.

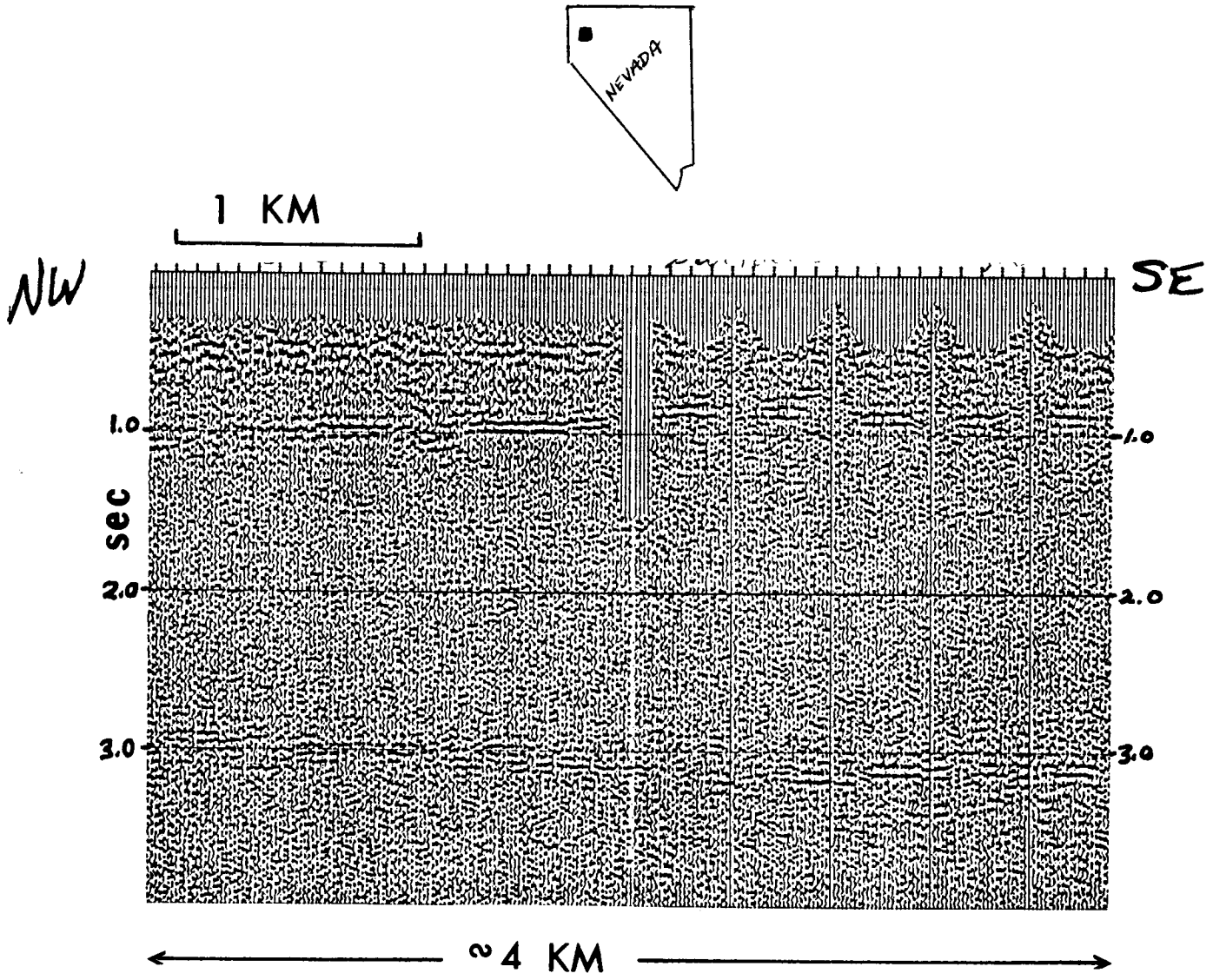

FIG. 2.19.

CONCLUSIONS

The migration of the COCORP Hardeman lines focused the deep-crustal seismic data such that interpretation became possible. The frequency-domain migration algorithm employed is fast, accurate, and appropriate in areas of stratified media with little lateral velocity variation, like Hardeman Cty. The migrated sections provide a more accurate picture of the crust because dipping events are shifted to their correct temporal and spatial locations (within the limits of a 2-D algorithm and dataset) and diffractions are collapsed. The signal/noise ratio is also improved. The interpretation of the COCORP profiles should be based on sections migrated with the proper algorithm.

The initial stacking velocity functions and the results of a later detailed velocity analysis by Schilt and Long (Cornell University) yielded the interval velocities which constrained the interpretation. Analysis of the resolution possible in the stacking velocities gave the error bars for the interval velocities. The analysis of dip recordability indicated that ***under*** the profiles, only gentle dips and flat events would be seen, due to the shortness of the lines. Sonic data from 2.56 km away validated the velocities of the sedimentary sequence. Igneous rock velocities came from laboratory data and sonic logs of Texas and Oklahoma wells penetrating considerable amounts of igneous rocks. Published seismic reflection work in this region added further insights. Regional velocities to Moho came from refraction work.

COCORP's Hardeman Cty. seismic experiment reveals what is interpreted as a silicic complex ~7.5 km thick, overlain by ~2.9 km of Paleozoic sediments. The top ~.6 km of the complex is porous tuff and flow, generating layered reflections, grading downward into 3.5 km of seismically transparent rhyolite/granite. The lower 3.2 km of the complex, between the two high-amplitude reflectors, is interpreted as silicic to intermediate plutonic rocks. The reflectivity of the two high-amplitude seismic events suggests mafic sills ~800 m thick, and the more reflective (thicker?) lens is at the base of the pluton. This tabular silicic

pluton is underplated by gabbroic rocks, rather than passing imperceptibly into migmatite. Our interpretation explains the subhorizontal nature of the two high-amplitude reflectors, the high reflection coefficient, and links the seismic data with the regional abundance of epizonal granite, rhyolite, and gabbro.

ACKNOWLEDGMENTS

Prof. Jon Claerbout and the Stanford Exploration Project provided the computer time, software, and hardware support for the migrations. A-lan von Hornlein helped with the research into possible mechanisms of batholith emplacement. Amoco very kindly provided the Pan Am. Bestwall Gypsum well data, which were invaluable. Assistance and information exchange with Cornell University's geophysics department and Petty-Ray Geophysical, Houston, is gratefully acknowledged. Gail Mahood kindly provided timely input and constructive criticism of the manuscript. Support for this research came in part from National Science Foundation Grant EAR 78-22762.

REFERENCES

Ahern, J.L., Turcotte, D.L., Oxburgh, E.R., 1979, On the upward migration of batholiths during solidification (abs.): EOS Transactions, v. 60, no. 18, p. 411.

Bailey, R.A., Dalrymple, G.B., and Lanphere, M.A., 1976, Volcanism, structure, and geochronology of Long Valley caldera, Mono County, Ca.: JGR, v. 81, p. 725-744.

Bateman, P.C., and Eaton, J.P., 1967, Sierra Nevada batholith: Science, v. 158, p. 1407-1417.

Bickford, M.E., Lewis, R.D., 1979, U-Pb geochronology of exposed basement rocks in Okla.: GSA Bull., v. 90, p. 540-544.

Birch, F., 1960, The velocity of compressional waves in rocks to 10 kilobars: JGR, v. 65, p. 1083-1102.

Callaway, James, 1978 Reflection seismic traverse across Black Rock Desert and Hualapai Flat, Nevada: Colo. School Mines Quarterly, v. 73, no. 3, p. 65-72.

Claerbout, J.F., 1976, Fundamentals of geophysical data processing: New York, McGraw-Hill.

Eichelberger, J.C., and Gooley, R., 1977, Evolution of silicic magma chambers and their relationship to basaltic volcanism: The Earth's Crust, AGU Mon. 20, p. 57-79.

Eichelberger, J.C., 1977, Andesitic volcanism and crustal evolution: Nature, v. 275, no. 5675, p. 21-27.

Flawn, P.T., 1956, Basement rocks of texas and southeast New Mexico: Texas Univ. Bur. Econ. Geol. Publ., no. 5605, 261 pages.
Flawn, P.T., and Muehlberger, W.R., 1970, The Precambrian of the USA: south-central US: The Precambrian, v. 4, K. Rankama, ed., p. 72-144.
Ham, W.E., Denison, R.E., and Merritr, C. A., 1964, Basement rocks and structural evolution of southern Okla.: Okla. Geol. Surv. Bull. 95, 302 pp.
Hamilton, W., and Myers, W.B., 1967, The nature of batholiths: Geol. Surv. Prof. Ppr. 554-C, 30 pp.
Hildreth, W., 1969, The Bishop Tuff: evidence for the origin of compositional zonation in silicic magma chambers: preprint for the GSA symposium volume on ash-flow tuffs.
Hyndman, D.W., 1972, Petrology of igneous and metamorphic rocks: McGraw-Hill.
Kjartansson, E., 1979, Ph.D. thesis, Stanford University.
Lachenbruch, A.H., Sass, J.H., Munroe, R.J., and Moses, T.H., Jr., 1976, Geothermal setting and simple heat conduction models for the Long Valley caldera: JGR, v. 81, no. 5, p. 769-784.
Lipman, P.W., 1966, Water pressures during differentiation and crystallization of some ash-flow magmas from southern Nevada: Amer. Jour. Sci., v. 264, p. 810-826.
Mayer, L., 1979, The origin of fine scale acoustic stratigraphy in deep sea carbonates: Jour. Geoph. Res., v. 84, p. 6177-6184.
Mitchell, B.J. and Landisman, M., 1970, Interpretation of a crustal section across Okla.: GSA Bull., v. 81, p. 2647-2656.
Morgan, B.A., 1970, Petrology and mineralogy of eclogite and garnet amphibolite from Puerto Cabello, Venezuela: Jour. of Petrol., v. 11, part 1, p. 101-145.
Muehlberger, W.R., Denison, R.E., and Lidiak, E.G., 1967, Basement rocks in continental interior of U.S.: AAPG, v. 51, no. 12, p. 2351-2380.
Oliver, J., Dobrin, M., Kaufman, S., Meyer, R., and Phinney, R., 1976, Continuous seismic reflection profiling of the deep basement: GSA Bull., v. 87, p. 1537-1546.
Oliver, J. and Kaufman, S., 1977, Complexities of the deep basement from seismic reflection profiling: The Earth's Crust, AGU Monograph 20, p. 243-253.
Roth, R., 1960, Swisher gabbroic terrane of the Tx. Panhandle: AAPG, v. 44, p. 1775-1784.
Schilt, S., Oliver, J., Brown, L., Kaufman, S., Albaugh, D., Brewer, J., Cook, F., Jensen, L. Krumhansl, P., Long, G., and Steiner, D., 1979, The heterogeneity of the continental crust: results from deep crustal seismic profiling using the VIBROSEIS technique:
Shaw, H.R., 1965, Comments on viscosity, crystal settling, and convection in granitic magmas: Amer. J. Sci., v. 263, p. 120-152.
Shaw, H.R., Wright, T.L., Peck, D.L., and Okamura, R., 1968, The viscosity of basaltic magma: an analysis of field measurements in Makaopuhi Lava Lake, Hawaii: Amer.J.Sci., v. 266, p. 225-264.
Smithson, S.B., Brewer, J., Kaufman, S., Oliver, J., and Hurich, C., 1979, Structure of the Laramide Wind River uplift, Wyo., from COCORP deep reflection data and from gravity data: Jour. Geophys. Res., v. 84, p. 5955-5972.
Stolt, R., 1978, Migration by Fourier transform: Geophysics, v. 43, p. 23-48.
Tex, E. den, and Vogel, D.E., 1962, A "Granulitgberg" at Cabo Ortegal

(NW Spain): Geol. Rundschau, v. 52, p. 95-112.
Tryggvason, E. and Qualls, B.R., 1967, Seismic refraction measurements of crustal structure in Okla.: JGR, v. 72, no. 14, p. 3738-3740.
Widdess, M.B., and Taylor, R.L., 1959, Seismic reflections from layering within the Precambrian basement complex, Okla.: Geophysics, v. 24, p. 417-425.
Yoder, H.S. Jr., 1976, Generation of basaltic magma: Washington D.C., National Academy of Sciences, 265 pp.

APPENDIX 1

Field Procedure (from Oliver et al., 1976).

Petty-Ray Geophysical, Inc., of Houston, Texas, was engaged for the data acquisition and computations. The field acquisition unit was a 48-channel MDS 8/Mandrel Data System; geophones were Electro-Technical Lab. EV22C with a natural frequency of 7.5 Hz; the VIBROSEIS technique was used, sources being five synchronized vibrators (three Y1100, each of 13.5 ton peak force, and two Y900, each of 10.5 ton peak force).

Two days were spent prior to production work to establish the field parameters. Studies of source-generated surface and near-surface waves were made using single location sources and podded [bunched] geophone spreads. Various arrays of vibrators and vibrator signal frequencies were studied. The parameters chosen for the production work were the following:

In-line source and geophone arrays.

Station spacing: 100 m (330 ft), geophone spread length 4.7 km (15,510 ft).

Distance of source station to nearest geophone: 400 m (1320 ft).

24 geophones per station, spread over a distance of 200 m (660 ft) (100 percent geophone overlap).

Vibrator array: (Y900 - Y1100 - Y1100 - Y1100 - Y900) vibrators 18.3 m (60 ft) apart, move-up interval of 6.5 m (20 ft); 16 sweeps summed per record.

Pilot signal: 15 sec duration; upsweep, 10 to 32 Hz.

8 msec sampling interval; 30 sec recording duration.

Normal vibrator locations were spaced two stations apart.

> The Hardeman County experiment was designed to provide data for 12-fold CDP stacking, and automatic gain control (AGC) was applied [on the original processing] to keep amplitudes relatively uniform as a function of time.

The original processing sequence was as follows: demultiplex, VIBROSEIS correlation using field sweep, velocity analysis, NMO with elevation correction to 1500 ft datum plane using a correctional velocity of 7000 ft/s, CDP gather, residual statics, 12 CDP stack, predictive deconvolution with a 320 msec operator and a ***fixed*** (***constant***) 72 msec lag, sliding window AGC using a 2400 msec window. This processing was applied to the data to produce the sections shown in Figures 2.2A, 2.3A, 2.4A.

On the reprocessing, true amplitude gain was applied to the gathers (Figure 2.5), and the stacked sections (Figures 2.2B, 2.3B, 2.4B) were AGC'd. The reprocessing sequence was as follows: demultiplex, VIBROSEIS correlate, CDP sort, NMO - mute - scale (AGC), residual statics, 12-fold CDP stack, predictive deconvolution with a 320 msec operator, with a second zero crossing lag, maximum lag permitted 72 msec, filter (5-10-30-45 Hz), scale [AGC]. The above reprocessing information is courtesy of F. Steve Schilt, Cornell Univ. and Roland Smith, Petty-Ray, Houston, Texas.

APPENDIX 2

Table A - D: original processing and reprocessing stacking velocity functions; interval velocities for all of the above.

The reprocessed velocities have two anomalous interval velocities. 8.7 and 9.2 km/s are not realistic for the upper crust (4-6 km depth). Such interval velocities exist because the stacking velocity was picked probably on a dipping event or a diffraction.

APPENDIX 2

TABLE A

Reprocessed Stacking Velocities,
Hardeman County, Texas, from Cornell University

Line		T (sec)	V (km/s)	Int. Vel. (km/s)		T (sec)	V (km/s)	Int. Vel. (km/s)
	Stns.	.65	3.35		Stns.	1.0	3.35	
1	1-20			4.35	100			4.2
		.9	3.65			1.5	3.65	
				4.5				5.98
		1.3	3.96			2.8	4.9	
				5.75				6.0
		1.52	4.27			3.7	5.18	
				5.9				7.07
		2.17	4.81			5.2	5.8	
				6.14				7.0
		2.9	5.18			6.3	6.02	
				6.5				6.9
		3.65	5.48			10.6	6.4	
				5.96				N.A.
		5.3	5.6			15.0	6.7	
				7.03				
		7.6	6.09					
		10.0	6.4	N.A.				
		15.0	6.7					
Line								
	Stns.	1.15	3.65		Stns.	1.0	3.35	
1	60			5.1	140-End			5.96
		1.4	3.96			1.4	4.27	
				5.55				5.95
		2.72	4.8			2.8	5.18	
				6.3				6.44
		3.7	5.2			3.6	5.48	
				6.6				7.15
		4.4	5.48			4.3	5.8	
				6.78				6.76
		7.9	6.09			6.1	6.09	
		15.0	6.7	N.A.		10.6	6.4	N.A.
						15.0	6.7	

APPENDIX 2

TABLE B

Reprocessed Stacking Velocities,
Hardeman County, Texas, from Cornell University

Line		T (sec)	V (km/s)	Int. Vel. (km/s)		T (sec)	V (km/s)	Int. Vel. (km/s)
	Stns.				Stns.			
2	1-45	.3	3.35		70-80			
				3.8				
		.7	3.65					
				3.6				
		1.3	3.65			1.4	3.65	
				6.38				5.6
		2.9	5.33			1.9	4.27	
				6.5				6.8
		3.8	5.6			2.75	5.18	
				6.6				6.2
		4.4	5.8			3.7	5.48	
				7.0				5.1
		7.2	6.09			4.9	5.6	
				N.A.				6.8
		15.0	6.8			7.6	6.09	
						15.0	6.7	N.A.

Line				
	Stns.			
2	100-End			
		1.05	3.65	
	Very			4.8
	good	1.35	3.96	
				5.9
		2.7	5.0	
				6.9
		2.9	5.18	
				6.4
		3.8	5.48	
				6.2
		4.8	5.8	
				7.04
		6.2	6.09	
		8.0	6.25	N.A.
		15.0	6.7	

APPENDIX 2

TABLE D

Initial Stacking Velocity Functions - Petty-Ray
Hardeman County, Texas

Vel. Fcn.	T (sec)	V (km/s)	Int. Vel. (km/s)
#10	0.0	1.83	
			3.7
(Line 3)	1.3	3.7	
			5.7
(End of line 2)	2.76	5.16	
			5.6
	6.1	5.4	
			6.45
	11.6	5.92	
			7.1
	14.	6.14	
	15.	6.82	N.A.

Vel. Fcn.	T (sec)	V (km/s)	Int. Vel.
#12	0.0	1.83	
			3.7
(Only at	1.3	3.7	
			6.8
end of line 1)	2.85	5.6	
			7.2
	4.27	6.22	
			6.6
	11.02	6.5	
			7.5
	14.	6.72	
	15.	6.8	N.A.

Vel. Fcn.	T (sec)	V (km/s)	Int. Vel.
#11	0.0	1.23	
			3.7
	1.3	3.7	
			5.8 ± .2
	2.4	4.8	
(1st 1/2			5.5 ± .4
line 2)	4.1	5.1	
			6.0 ± .6
(1st 1/2	6.1	5.4	
line 1)			6.45
	11.6	5.92	
			7.1
	14.0	6.14	
	15.0	6.8	N.A.

APPENDIX 3

Velocity resolution discrimination method

A given stacking velocity indicates a specific NMO correction for the farthest live offset. (The muting, or gating, function must be part of the input.) When that offset's moveout is varied by ± 1 sample, a slower/faster stacking velocity is indicated. Picking the moveout correction to within ± 1 sample is considered a limit imposed by the sample rate to the velocity resolution attainable (especially late in time). This analysis was suggested by D.Y. LeCorgne.

The equation used in this analysis is simply the NMO equation:

$$(T_o)^2 + (\frac{F}{V_{stk}})^2 = (T_F)^2 = (T_o + \Delta t)^2$$

where T_o = the time of the event on the near trace, F = the farthest live offset, T_F = the time of the event at the offset, V_{stk} = the stacking velocity, and Δt = the normal moveout correction. Given V = V(t) and F = F(t), Δt is calculated. Δt is then altered by one sample, and V(t) is recalculated for the two different NMO corrections.

Once lower and upper bounds of resolution are set for the stacking velocities, analysis of the interval velocity resolution may be undertaken.